JCB Journal of Cell Biology

ARTICLE

Loss of myosin Vb promotes apical bulk endocytosis in neonatal enterocytes

Amy C. Engevik[1,2], Izumi Kaji[1,2], Meagan M. Postema[2], James J. Faust[2], Anne R. Meyer[2], Janice A. Williams[1,3], Gillian N. Fitz[2], Matthew J. Tyska[2,3], Jean M. Wilson[5], and James R. Goldenring[1,2,3,4]

In patients with inactivating mutations in myosin Vb (Myo5B), enterocytes show large inclusions lined by microvilli. The origin of inclusions in small-intestinal enterocytes in microvillus inclusion disease is currently unclear. We postulated that inclusions in Myo5b KO mouse enterocytes form through invagination of the apical brush border membrane. 70-kD FITC-dextran added apically to Myo5b KO intestinal explants accumulated in intracellular inclusions. Live imaging of Myo5b KO–derived enteroids confirmed the formation of inclusions from the apical membrane. Treatment of intestinal explants and enteroids with Dyngo resulted in accumulation of inclusions at the apical membrane. Inclusions in Myo5b KO enterocytes contained VAMP4 and Pacsin 2 (Syndapin 2). Myo5b;Pacsin 2 double-KO mice showed a significant decrease in inclusion formation. Our results suggest that apical bulk endocytosis in Myo5b KO enterocytes resembles activity-dependent bulk endocytosis, the primary mechanism for synaptic vesicle uptake during intense neuronal stimulation. Thus, apical bulk endocytosis mediates the formation of inclusions in neonatal Myo5b KO enterocytes.

Introduction

Defects in endocytosis and trafficking are implicated in a number of neonatal diseases, including microvillus inclusion disease (MVID; Knowles et al., 2014; Cox et al., 2017). MVID is a rare congenital disorder that results in life-threatening diarrhea and malnutrition in neonates (Davidson et al., 1978; Ruemmele et al., 2006). Mutations in the processive motor protein myosin Vb (Myo5b) are the primary drivers of MVID (Pohl et al., 1999; Erickson et al., 2008; Müller et al., 2008; Ruemmele et al., 2010; Szperl et al., 2011; Golachowska et al., 2012). Patients with MVID manifest enterocyte abnormalities, which includes subapical inclusions lined with discrete microvilli and decreased expression of apical nutrient transporters (Cutz et al., 1989; Ruemmele et al., 2006; Knowles et al., 2014; Engevik et al., 2018). To better understand the molecular mechanisms that underpin MVID, several laboratories, including our own, have created mouse models that recapitulate the major phenotypes of MVID patients (Cartón-García et al., 2015; Schneeberger et al., 2015; Weis et al., 2016; Engevik et al., 2018). Of note, we found that germline Myo5b knockout (KO) mice display prominent microvillus inclusions in the duodenal mucosa, and induction of Myo5b KO in intestine-specific inducible KO mice during the neonatal period also induces inclusion formation (Weis et al., 2016). Induction of Myo5b KO in adult mice produces 10-fold fewer inclusions. These findings have led to the suggestion that neonatal-specific processes account for the development of inclusions after inactivation of Myo5b.

Currently, the origins of inclusions in patients with MVID remain contentious, as well as whether they result from endocytosis or exocytosis. Reinshagen et al. (2002) reported that microvillus-lined inclusions formed through autophagocytosis of the apical brush border of enterocytes from MVID patient biopsies. In that study, organ cultures from MVID patients demonstrated internalization of cationized ferritin and ovalbumin, providing experimental evidence for involvement of an endocytic pathway in the formation of microvillus inclusions. Rab8a-deficient mice display features of MVID including diarrhea, shortened microvilli, and inclusions in the small intestine (Sato et al., 2007). Feeding of fluid-phase marker (FITC-IgG) to 3-wk-old Rab8a KO mice demonstrated that inclusions in these mice arose from endocytosis, since FITC-IgG was present intracellularly in F-actin–ringed inclusions in enterocytes (Sato et al., 2007). Similarly, using germline Myo5b KO mice, our laboratory previously reported the presence of maternal IgG in intracellular inclusions, suggesting that inclusions formed from

[1]Department of Surgery, Vanderbilt University School of Medicine, Nashville, TN; [2]Department of Cell and Developmental Biology, Vanderbilt University School of Medicine, Nashville, TN; [3]The Epithelial Biology Center and Vanderbilt University School of Medicine, Nashville, TN; [4]The Nashville VA Medical Center, Nashville, TN; [5]Department of Cellular and Molecular Medicine, Bio5 Institute, University of Arizona, Tucson, AZ.

Correspondence to James R. Goldenring: jim.goldenring@vanderbilt.edu.

internalization of the apical membrane of enterocytes (Weis et al., 2016). In intestinal organoids derived from syntaxin binding protein 2–null mice, Mosa et al. (2018) observed microvillus inclusion formation both de novo in the cytoplasm and through internalization of the apical or basolateral plasma membrane. Loss of function mutations in syntaxin binding protein 2 result in familial hemophagocytic lymphohistiocytosis type 5, a disease that manifests gastrointestinal symptoms similar to MVID (Davidson et al., 1978; Côte et al., 2009; Pagel et al., 2012; Stepensky et al., 2013; Vogel et al., 2017; Mosa et al., 2018). Silencing of the V0-ATPase in *Caenorhabditis elegans* also revealed microvillus inclusion formation de novo in the cytoplasm or from internalization of large structures from the apical or basolateral plasma membrane (Bidaud-Meynard et al., 2019). The formation of microvillus-lined inclusions, best characterized in MVID, has been postulated to arise from nucleation in the cytoplasm or from internalization of the plasma membrane (Davidson et al., 1978; Cutz et al., 1989; Mosa et al., 2018; Bidaud-Meynard et al., 2019).

Previous studies relying on human tissue from MVID patients observed that only 10–20% of enterocytes contain inclusions (Cutz et al., 1989). We postulate that this may be due to the developmental stage of patients with fewer inclusions being present in older patients than in neonatal patients. In support of this, our group and Schneeberger et al. (2015) both reported few inclusions in adult-inducible VilCre^{ERT2};Myo5b$^{fl/fl}$ mice following tamoxifen administration (Weis et al., 2016). In contrast, induction of Myo5b loss in neonatal VilCre^{ERT2};Myo5b$^{fl/fl}$ mice resulted in numerous inclusions (Weis et al., 2016). Tamoxifen-inducible VilCre^{ERT2};Myo5b$^{fl/fl}$ mice and germline Myo5b KO mice all exhibit defects in apical brush border protein trafficking (Cartón-García et al., 2015; Schneeberger et al., 2015; Weis et al., 2016; Engevik et al., 2018). These findings indicate that formation of inclusions may not account for defects in delivery of apical transporters to the brush border.

The limited amount of human tissue available from MVID patients complicates experimental approaches to understand the dynamics of inclusion formation. Additionally, sole use of adult mice or intestinal enteroids/organoids to model inclusion formation may not fully recapitulate developmental processes that likely contribute to inclusion formation. In this investigation, we use germline Myo5b KO mice to demonstrate in vivo, ex vivo, and in vitro inclusion formation by apical endocytosis in small-intestinal enterocytes. Our experiments demonstrate that inclusions are formed from bulk endocytosis of the brush border of enterocytes. Analysis of Myo5b KO mouse small-intestinal tissue showed large inclusions lined by microvilli that were surrounded by the endosomal protein, endotubin. Addition of 70-kD fluorescent dextran to the apical domain of intestinal explants of Myo5b KO mouse small intestine resulted in F-actin–positive inclusions that contained fluorescently conjugated dextran. Inclusion formation by bulk endocytosis is a slow process in Myo5b KO mouse enterocytes, occurring over several hours. Bulk endocytosis that results from loss of Myo5b was found to be dependent on dynamin and Pacsin 2. Moreover, inclusions formed by apical bulk endocytosis in Myo5b KO mice are characterized as being positive for vesicle-associated membrane protein 4 (VAMP4) and Pacsin 2 and are associated with Dynamin 2 complexes. These findings suggest that apical bulk endocytosis in neonatal Myo5b KO mice has similarities with a neuronal endocytic pathway termed activity-dependent bulk endocytosis (ADBE). ADBE results in the internalization of large quantities of cell membrane following intense neuronal stimulation in the central nervous system (Takei et al., 1996; Richards et al., 2000; Clayton et al., 2008). Collectively, our data indicate that loss of Myo5b from neonatal enterocytes results in activaton of a previously uncharacterized pathway, apical bulk endocytosis, which resembles ADBE.

Results

Loss of Myo5b results in intracellular inclusions surrounded by endotubin

To characterize the formation of inclusions, we analyzed the proximal small intestine (duodenum and jejunum) of neonatal control and germline Myo5b KO mice. Immunostaining demonstrated that inclusions in neonatal germline Myo5b KO mice were positive for apical membrane markers such as the brush border enzyme dipeptidyl peptidase (DPPIV) and the actin-linking protein, ezrin, as reflected by staining for phosphorylated ezrin-radixin-moesin (P-ERM; Fig. 1, A and B). Immunostaining for the apical endosome protein, endotubin, showed endotubin present immediately below the brush border as marked by P-ERM in neonatal control mice (Fig. 1, C and D). In Myo5b KO mice, endotubin was frequently absent from its normal location in the tubular apical endosome below the brush border. Many inclusions in Myo5b KO mice were closely associated with endotubin (Fig. 1 C). Interestingly, inclusions still attached to the brush border appeared to be encircled by endotubin (Fig. 1 D).

Inclusion formation in Myo5b KO mice results from internalization of the brush border in enterocytes

To identify whether inclusions form through endocytosis, we performed explant experiments. Germline Myo5b KO mice were crossed with transgenic mice expressing LifeAct fused to eGFP (termed LifeAct mice) to visualize F-actin in the brush border of enterocytes. The duodenum of control LifeAct and Myo5b KO;LifeAct mice was excised and imaged to analyze subapical inclusions in three dimensions. Control LifeAct mice (Fig. 2 A) and Myo5b KO;LifeAct (Fig. 2 B) mice showed fluorescent labeling of the microvilli forming the brush border. Z-stack projections of control LifeAct mice showed small subapical actin-rich structures below the brush border (Fig. 2 A). In contrast, Myo5b KO;LifeAct mice showed large intracellular actin-rich spherical vesicles or inclusions (Fig. 2 B). To test whether microvillus inclusions were forming via endocytosis, proximal small-intestine (duodenum and jejunum) explants from control and Myo5b KO mice were mounted in Üssing chambers to provide oxygenated media to maintain the tissue integrity for 4 h. 70-kD FITC-dextran was added to the apical side of control and Myo5b KO tissue to determine whether the high molecular weight dextran would be incorporated into enterocytes. Previous investigations have demonstrated that 70-kD dextran is not taken up by clathrin-dependent endocytosis but is incorporated into

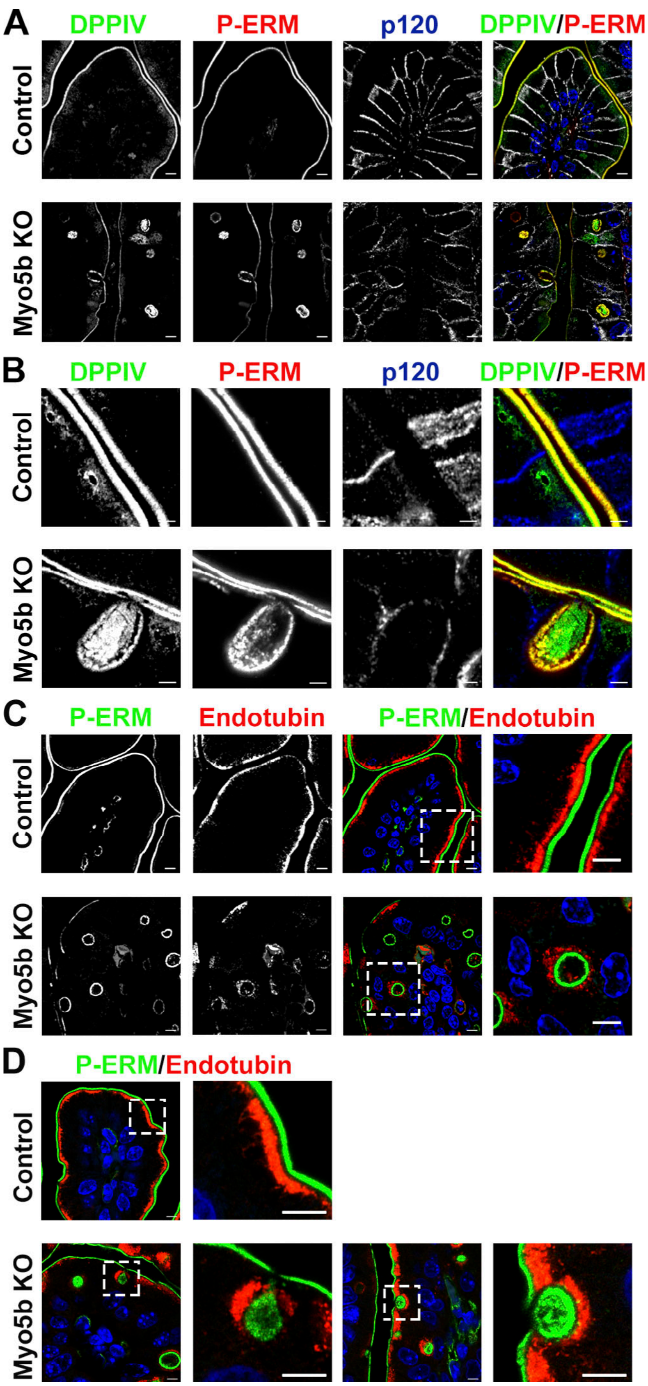

Figure 1. **Presence of large microvilli-lined inclusions contain apical membrane components in Myo5b KO mice. (A and B)** Immunostaining for the apical protein P-ERM (red) and the brush border enzyme DPPIV (green) showed apical localization in control mice. Myo5b KO mice exhibited numerous P-ERM–positive inclusions, many of which contained DPPIV. The basolateral protein p120 (white) delineates individual cells. Scale bars = 5 µm. **(B)** High-magnification image shows close association of inclusions with the apical membrane and internalized DPPIV. **(C)** The apical endosomal protein endotubin (red) normally localizes to tubular endosomes of the apical endosome complex immediately below the enterocyte brush border of neonatal control mice. In Myo5b KO enterocytes, endotubin can be seen surrounding numerous large intracellular inclusions. Scale bars = 2 µm. **(D)** Endotubin is closely associated with multiple inclusions that remain contiguous with the apical membrane in Myo5b KO enterocytes. Scale bars = 5 µm. *n* = 6 mice per group.

cells by macropinocytosis (Li et al., 2015). No F-actin–positive inclusions were identified in control mice. However, 70-kD FITC-dextran was observed in a number of enterocytes, suggesting that the neonatal intestine may be actively taking up luminal contents through a bulk endocytosis mechanism (Fig. 2 C). Nevertheless, Myo5b KO mice showed numerous F-actin–positive inclusions, many of which contained fluorescent dextran (Fig. 2 D). These findings indicate that inclusions in Myo5b KO enterocytes are forming through bulk endocytosis from the apical membrane.

Enteroids derived from Myo5b KO mice form intracellular inclusions through endocytosis

We next sought to confirm the formation of inclusions via bulk endocytosis using the reductionist model of enteroids derived from the proximal small intestine of neonatal control and Myo5b KO mice. Hematoxylin and eosin (H&E) micrographs of enteroids show similar gross morphology between control and Myo5b KO–derived enteroids (Fig. 3 A). However, transmission EM (TEM) images demonstrate decreased height of microvilli in Myo5b KO enteroids compared with enteroids generated from control mice (Fig. 3 A). This is consistent with findings from the small intestine of Myo5b KO mice, which showed shorter and thicker microvilli lining the apical membrane (Weis et al., 2016). Myo5b KO enteroids also had numerous intracellular inclusions lined with microvilli, similar to observations in the native intestinal tissue of Myo5b KO mice (Weis et al., 2016; Fig. 3 A). In the Myo5b KO enteroids, TEM revealed a microvillus-lined inclusion immediately below the apical membrane that is denuded of microvilli. The subapical inclusion appears to have arisen from the apical membrane, where the microvilli were likely internalized from the brush border (Fig. 3 A). Immunofluorescence staining for P-ERM also confirmed the presence of numerous inclusions in Myo5b KO enteroids (Fig. 3 A).

To identify the dynamics of apical bulk endocytosis, we performed live imaging of enteroids from Myo5b KO;LifeAct mice to visualize inclusion formation in real time (Figs. 4 and S1). Enteroids from control mice showed a stable brush border and no inclusion formation (Fig. S1 and Video 1). In contrast, live imaging of enteroids from Myo5b KO;LifeAct mice showed inclusion formation from internalization of the apical membrane (Fig. 4 and Video 2). Analysis of formation of multiple inclusions showed that internalization of inclusions occurred over 90–220 min.

To characterize the mechanism of inclusion formation, enteroids were treated for 4 h with a variety of inhibitors (Fig. 3 B). Dynamin 1 is expressed in neurons and plays a crucial role in vesicle fission (De Camilli et al., 1995). Dynamin 2 is ubiquitously expressed and is highly expressed in the gastrointestinal tract (Uhlén et al., 2015; see Human Protein Atlas, http://www.proteinatlas.org). The dynamin inhibitor Dyngo or DMSO (0.1% vol/vol) as vehicle was added to enteroid medium to determine whether inclusion internalization was arrested (Fig. 3 B). In control enteroids, no effect was observed (Fig. S2). However, in enteroids derived from Myo5b KO mice, treatment with Dyngo resulted in a significant increase in inclusions that remained attached to the apical membrane (Fig. 3, B and C). These

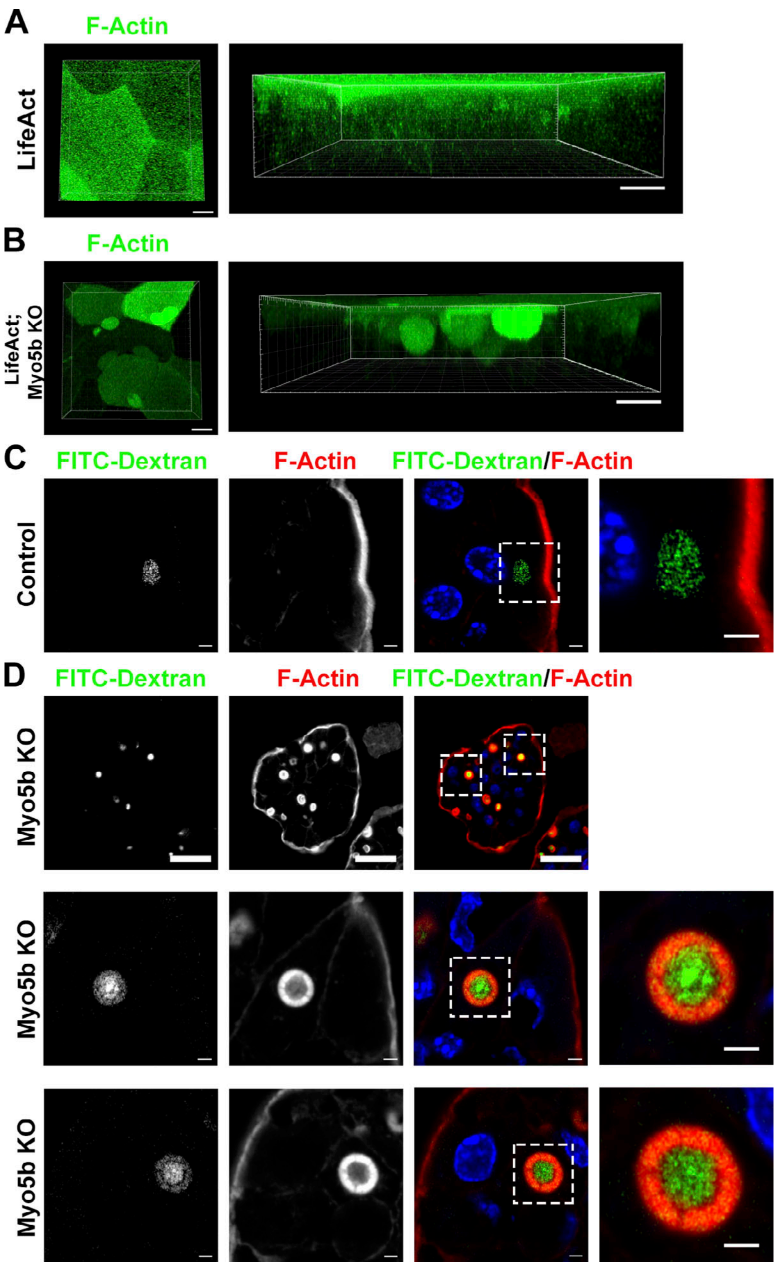

Figure 2. **Inclusion formation following loss of Myo5b results from endocytosis of the brush border. (A and B)** Myo5b KO mice were crossed with LifeAct mice expressing fluorescent F-actin to allow for visualization of the brush border and inclusion formation. **(A)** Live explants of control LifeAct mice showed moderate subapical expression of F-actin (green). **(B)** LifeAct;Myo5b KO mice had large F-actin–rich inclusions, many of which appeared to be attached to the apical membrane. Scale bars = 10 µm. **(C and D)** To determine whether inclusions form through endocytosis of the brush border, 70-kD FITC-dextran was added to the apical side of proximal small-intestine explants (duodenum and jejunum) from neonatal control (C) and Myo5b KO mice (D). Scale bars = 25 µm for first panel of C (low-magnification image). In control mice, no subapical F-actin–positive inclusions were observed; however, a small number of cells had FITC-dextran accumulation (C). In Myo5b KO enterocytes, numerous F-actin inclusions were observed containing concentrated FITC-dextran, providing evidence that inclusions form via endocytosis (D). *n* = 3–5 mice per group (groups: LifeAct, LifeAct;Myo5b KO, control, and Myo5b KO). Scale bars for C and D = 2 µm.

results suggest that dynamin is essential for the fission of inclusions from the apical domain. 5-(*N*-ethyl-*N*-isopropyl)-amiloride (EIPA) was also administered to enteroids to determine whether inclusion formation was proceeding via macropinocytosis (Ivanov, 2008; Koivusalo et al., 2010; Commisso et al., 2013). EIPA had no effect on the abundance of inclusions in Myo5b KO enteroids or on the prevalence of inclusions at the apical membrane (Fig. 3 B). The protein phosphatase calcineurin has previously been reported to be an inhibitor of ADBE after neuronal hyperstimulation (Cheung et al., 2010). To determine the effects of calcineurin on bulk endocytosis of the apical membrane in Myo5b-deficient enterocytes, cyclosporin A (an inhibitor of calcineurin; Azzi et al., 2013) was administered to enteroids. Treatment with cyclosporin A did not result in a significant increase in percentage of inclusions that remained at the apical membrane in Myo5b KO mice (Fig. 3, B and C). However, administration of cyclosporin A resulted in a significant decrease in total number of inclusions in Myo5b KO–derived enteroids (Fig. 3 D). These findings suggest that loss of Myo5b in neonatal enterocytes results from apical bulk endocytosis that requires the calcium-dependent protein phosphatase calcineurin and dynamin for inclusion formation, fission, and ultimately internalization of the apical membrane.

Treatment of intestinal explants with Dyngo results in accumulation of inclusions at the apical membrane

Immunostaining for Dynamin 2 was performed to determine the localization of Dynamin 2 in neonatal control and Myo5b KO mice. In control enterocytes, Dynamin 2 was expressed immediately below the brush border delineated by DPPIV and above endotubin (Fig. 5 A). In Myo5b KO mice, Dynamin 2 was concentrated in discrete locations associated with inclusions,

https://doi.org/10.1083/jcb.201902063

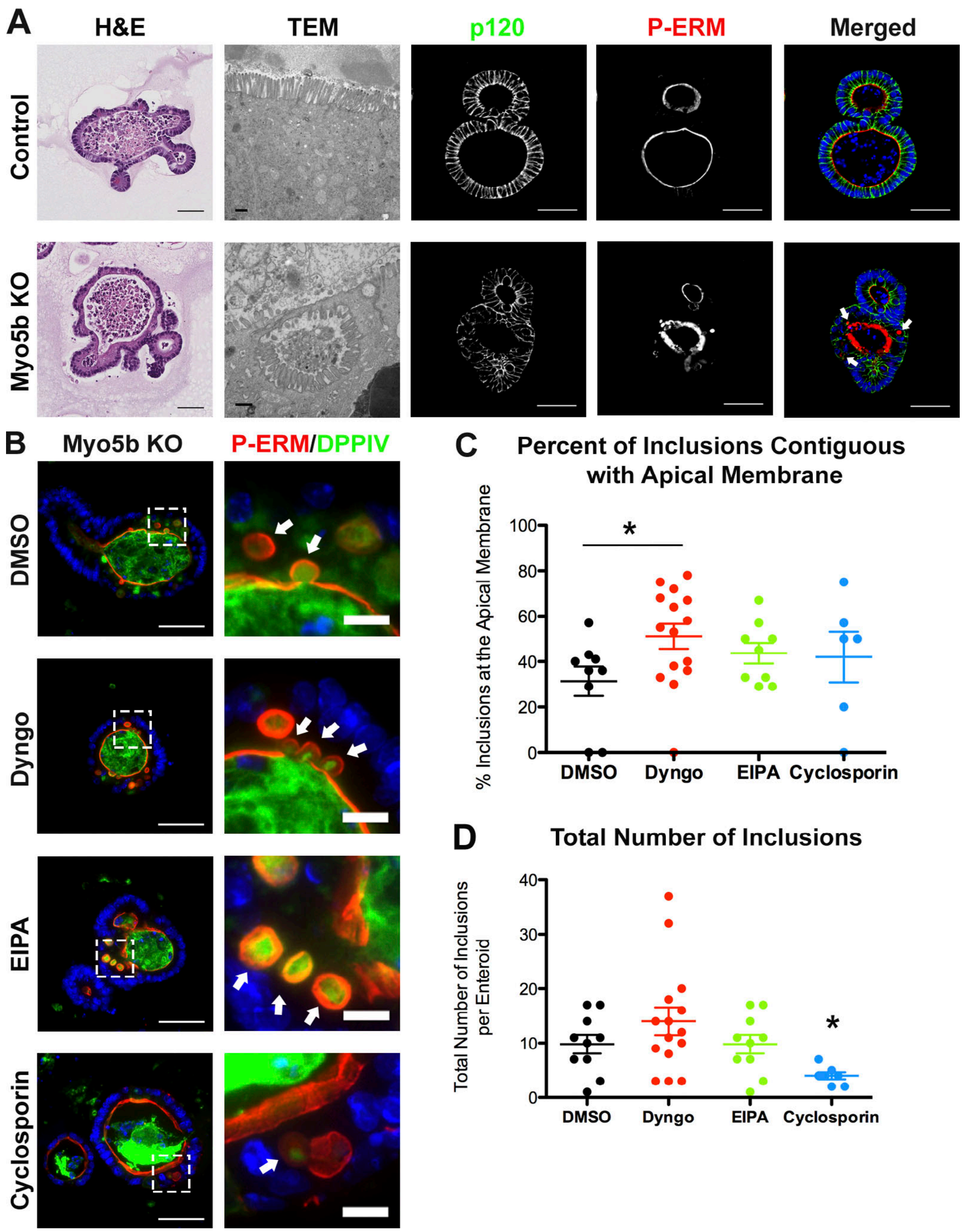

Figure 3. **Enteroids derived from Myo5b KO mice form inclusions via apical bulk endocytosis. (A)** H&E staining and TEM of enteroids derived from the duodenum of neonatal control and Myo5b KO mice. Morphologically, enteroids from control and Myo5b KO appeared similar; however, TEM revealed the presence of large intracellular inclusions lined with microvilli in Myo5b KO enteroids. Immunofluorescence staining showed the presence of numerous P-ERM–positive (red) inclusions in Myo5b KO–derived enteroids. H&E scale bars = 50 µm, TEM scale bars = 500 nm, immunofluorescence micrograph scale bar = 50 µm. **(B)** Enteroids generated from Myo5b KO mice were treated with DMSO (vehicle), Dyngo, EIPA, and cyclosporin to determine the mechanism of inclusion formation. P-ERM (red) and DPPIV (green) staining showed the presence of numerous inclusions, some still contiguous with the apical membrane in Myo5b KO enteroids. Arrows indicate the positions of inclusions. **(C)** The number of inclusions attached to the apical membrane and the total number of inclusions present in individual enteroids was quantified. The percentage of inclusions associated with the brush border in enteroids was then calculated, and the percentage of inclusions contiguous with the apical membrane in each individual enteroid was plotted. With administration of Dyngo, there was a significant increase in the percentage of inclusions that were still attached to the apical membrane compared with DMSO-treated enteroids. **(D)** The total number of inclusions was quantified in individual Myo5b KO enteroids to address whether treatments (Dyngo, EIPA, or cyclosporin) impacted inclusion formation. Administration of cyclosporin resulted in a significant decrease in inclusion formation in Myo5b KO enteroids. Scale bars = 50 µm for left panel of B, 10 µm for right panel of B. Enteroids were generated from three to five control and Myo5b KO mice. n = 6–15 enteroids analyzed per treatment; *, $P < 0.05$. One-way ANOVA was performed with the Bonferroni post hoc test for C and D; error bars are SEM.

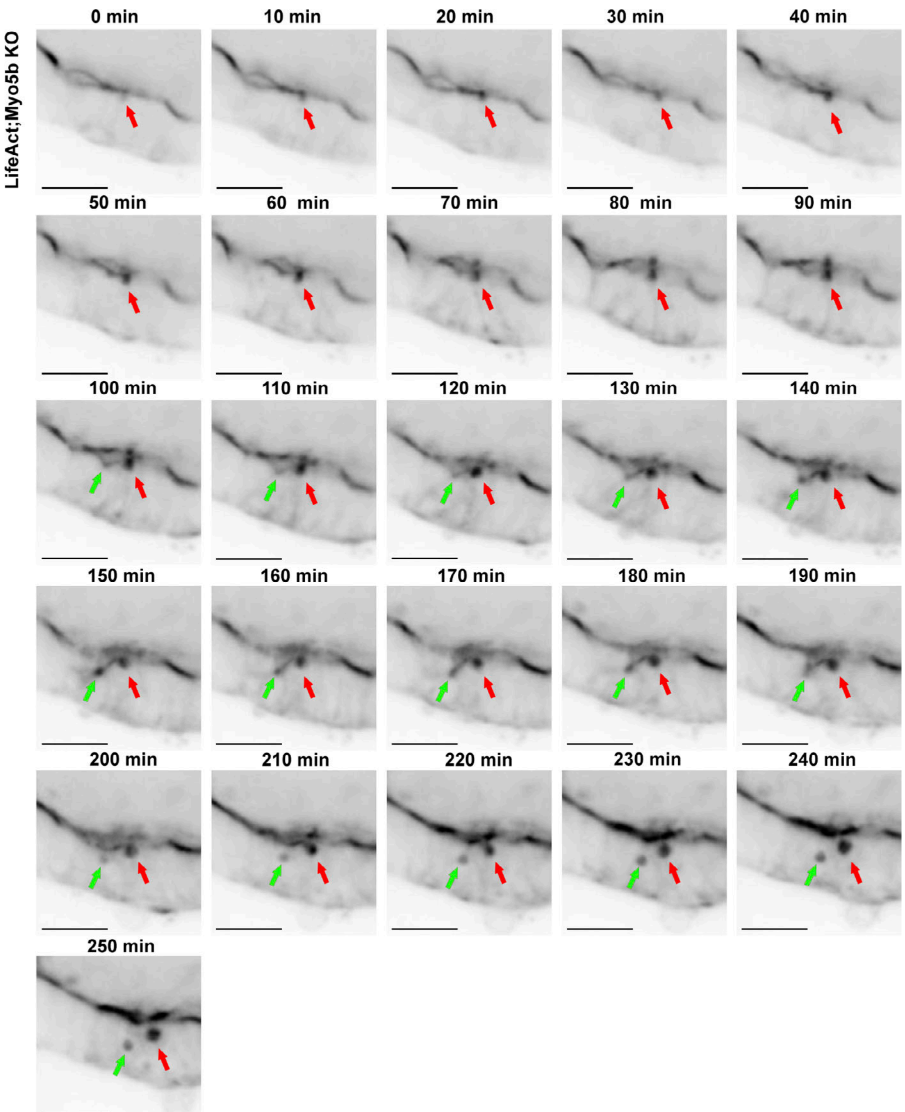

Figure 4. **Live imaging of LifeAct;Myo5b KO–derived enteroids showed inclusion formation through endocytosis of the apical membrane.** Enteroids generated from the proximal small intestine (duodenum) of neonatal LifeAct;Myo5b KO mice were imaged overnight at 37°C with 5% CO_2 to examine whether inclusions formed from internalization of the apical membrane. Confocal imaging of LifeAct;Myo5b KO–derived enteroids showed inclusions (red and green arrows) forming from endocytosis of the brush border followed by internalization into enterocytes. Scale bars = 25 µm.

identified as containing DPPIV and surrounded by endotubin (Fig. 5 B). We observed several different orientations of Dynamin 2 expression in Myo5b KO enterocytes. Inclusions that appeared to be forming through invagination of the apical membrane had Dynamin 2 concentrated at the neck of the inclusion. In fully internalized inclusions, we observed large accumulations of Dynamin 2 that remained associated with inclusions. We also observed more than one Dynamin 2 complex associated with an individual inclusion.

Explants from the proximal small intestine (duodenum and jejunum) of control and Myo5b KO mice were treated with DMSO or Dyngo for 4 h to determine if inhibition of dynamin resulted in failure of inclusion excision from the apical membrane. Intestinal explants from littermate control mice showed no changes with Dyngo treatment (Fig. 6 A). Myo5b KO explants showed a significant increase in the number of omega structures that remained at the apical membrane when treated with Dyngo (Fig. 6, A and B). Addition of 70-kD FITC-dextran to explants treated with DMSO or Dyngo demonstrated a significant decrease in internalization of FITC-dextran in the Myo5b KO mouse tissue treated with Dyngo (Fig. 6 C). In DMSO-treated Myo5b KO explants, ~20% of inclusions contained FITC-dextran. The uptake of dextran likely represents internalization into the inclusions that were actively forming over the 4-h incubation with FITC-dextran. These data suggest that dynamin plays an essential role in intracellular inclusion formation from bulk endocytosis following loss of Myo5b.

Inclusion formation occurs through apical bulk endocytosis in Myo5b KO enterocytes

During intense neuronal stimulation, a process of bulk endocytosis occurs to rapidly retrieve synaptic vesicles (Clayton and Cousin, 2009). This synaptic vesicle retrieval mode in the brain is known as ADBE (Royle and Lagnado, 2003; Rizzoli and Betz, 2005; Wu et al., 2007; Clayton et al., 2008). We postulated that a similar mechanism, referred to as apical bulk endocytosis, is occurring during inclusion formation and internalization in the neonatal small intestine of Myo5b KO mice. VAMP4 is essential for endocytosis of synaptic vesicles during ADBE (Nicholson-Fish et al., 2015). To determine whether VAMP4 is

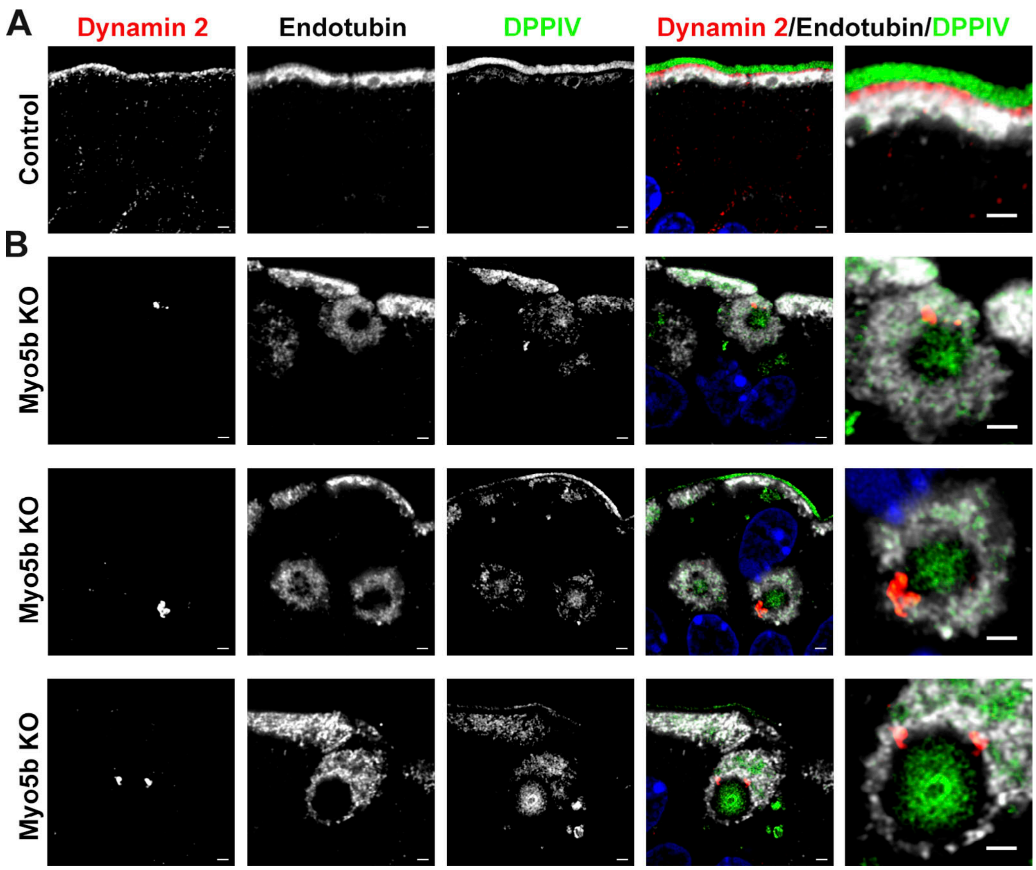

Figure 5. **Dynamin 2 association with inclusion formation in Myo5b KO mice. (A)** Immunostaining for Dynamin 2 (red) in the duodenum of neonatal control mice showed that Dynamin 2 was concentrated below the apical brush border as demarcated by DPPIV (green). The endosomal protein endotubin appeared to be localized immediately below Dynamin 2 in enterocytes. **(B)** In Myo5b KO enterocytes, Dynamin 2 appeared to concentrate with inclusions that were DPPIV and endotubin positive. In inclusions near the apical membrane, Dynamin 2 was evident in regions where detachment from the apical membrane appeared to be occurring. In fully internalized inclusions, Dynamin 2 was still associated with inclusions, frequently in distinct aggregates. Interestingly, two or more discrete Dynamin 2 regions were often observed in association with a single inclusion. *n* = 6 mice per group. Scale bars = 5 µm.

an endocytic cargo in the neonatal small intestine, we performed immunostaining for VAMP4. In the proximal small intestine of control mice, we observed VAMP4 on the apical membrane of enterocytes (Fig. 7 A). In Myo5b KO mice, VAMP4 was still present on the brush border, but enterocytes also exhibited numerous VAMP4-positive intracellular inclusions. Many inclusions were double positive for VAMP4 and DPPIV (Fig. 7 A).

Next we performed immunostaining for the endocytosis accessory protein and actin remodeler, Pacsin 2 (Syndapin 2; Roos and Kelly, 1998; Ritter et al., 1999; Simpson et al., 1999; Qualmann and Kelly, 2000; Dharmalingam et al., 2009; Rao et al., 2010). Syndapin 1 is involved in endocytosis for synaptic vesicle recycling in neurons (Qualmann and Kelly, 2000). Syndapin 1 is expressed in the central nervous system, while Pacsin 2 is ubiquitously expressed throughout the body. In control mice, Pacsin 2 was robustly expressed in the brush border of the proximal small intestine (duodenum and jejunum; Fig. 7 B). In Myo5b KO small intestine, Pacsin 2 showed decreased expression at the apical membrane but was present in numerous intracellular inclusions (Fig. 7 B). These findings suggested that Pacsin 2 participates in apical bulk endocytosis following loss of Myo5b in the neonatal small intestine, similar to its involvement in ADBE in the nervous system. Quantification of Pacsin 2–positive inclusions showed that, among inclusions containing DPPIV, ~40% also contained Pacsin 2 (Fig. S3). Interestingly, P-ERM–, endotubin-, and Pacsin 2–containing inclusions all represented ~40% of inclusions (as defined as DPPIV positive) in Myo5b KO mice. VAMP4-positive inclusions accounted for ~60% of inclusions in the proximal small intestine of Myo5b KO mice.

To determine whether Pacsin 2 was essential for apical bulk endocytosis, Myo5b KO mice were crossed with Pacsin 2 KO mice to achieve Myo5b KO;Pacsin 2 KO (double KO) mice. Mice lacking both Myo5b and Pacsin 2 still manifested many of the same small-intestinal defects seen in Myo5b KO mice, including fused villi, abnormal distribution of components of the brush border, and early demise (Figs. 8 A and S4). Interestingly, quantitation of inclusions in the proximal small intestine (duodenum and jejunum) showed a significant decrease in inclusions in Myo5b KO;Pacsin 2 KO mice compared with Myo5b KO mice (Fig. 8, B and C). Collectively, these data suggest that Pacsin 2 is required for inclusion formation in the setting of loss of Myo5b. Additionally, fewer inclusions did not ameliorate the intestinal defects in apical protein trafficking and expression in the brush

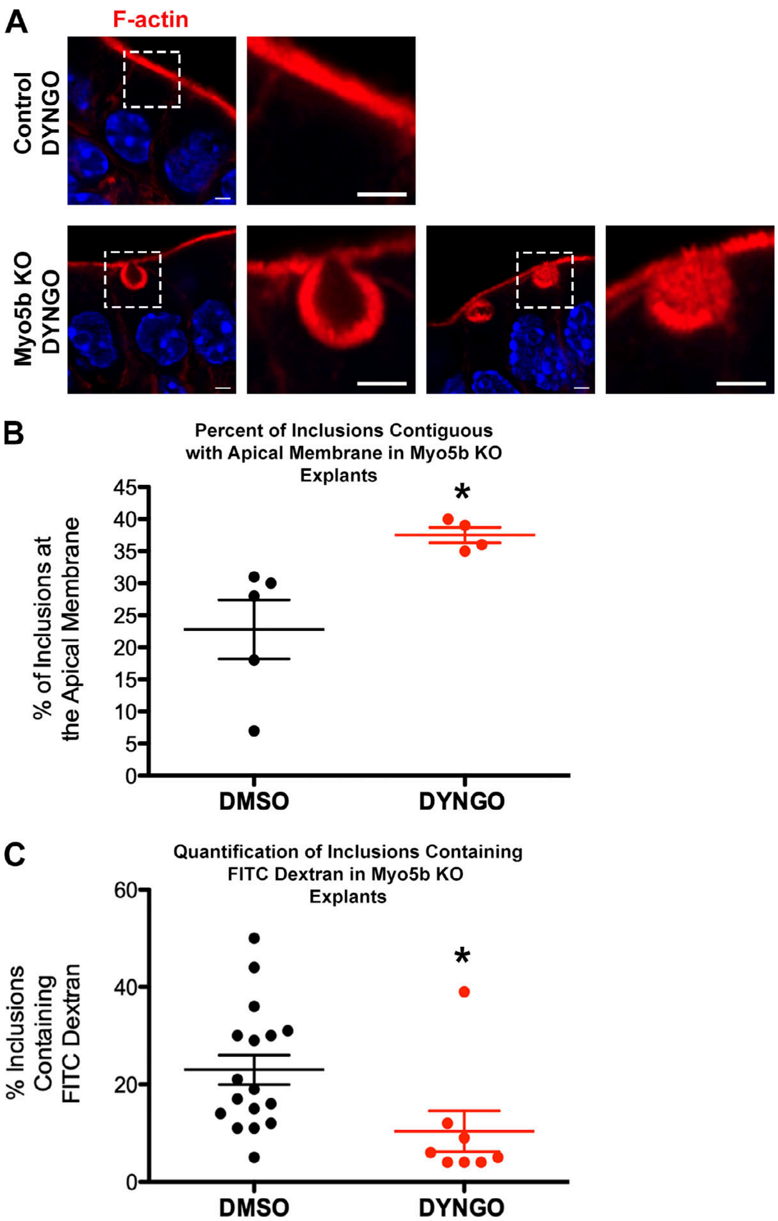

Figure 6. **Treatment of Myo5b KO intestinal explants with Dyngo resulted in an increase in inclusions contiguous with the apical membrane. (A)** Two to four pieces of small-intestinal tissue (duodenum and jejunum) were mounted from each mouse into individual Üssing chambers to ensure tissue viability of explants. In small-intestinal explants from control mice, no inclusion formation was observed at the apical membrane after 4 h of incubation with Dyngo (n = 5 control mice). In Myo5b KO intestinal explants, administration of Dyngo resulted in numerous F-actin–rich (red) inclusions that failed to excise from the apical membrane (n = 4 Myo5b KO mice). Scale bars = 5 µm. **(B)** The percentage of inclusions attached to the apical membrane of enterocytes of Myo5b KO mice treated with DMSO (vehicle) and Dyngo was calculated by counting the number of inclusions contiguous with the apical membrane and the total number of inclusions in individual mice (n = 4 Dyngo-treated Myo5b KO mice and n = 5 DMSO-treated Myo5b KO mice). Treatment with Dyngo resulted in significantly more inclusions remaining at the apical membrane in Myo5b KO explants. **(C)** To confirm a decrease in internalization of inclusions in Myo5b KO mouse explants treated with Dyngo, 70-kD FITC-dextran was added to the apical media of each explant treated in the presence of Dyngo or DMSO. The percentage of inclusions containing FITC-dextran in each explant treated with DMSO or Dyngo was calculated by quantifying FITC-dextran–positive inclusions and total inclusions. Addition of FITC-dextran to the apical media of each explant resulted in fewer inclusions containing FITC-dextran in Myo5b KO explants treated with Dyngo. *, $P < 0.05$. One-sided Student's t test was performed for B and C; error bars are SEM.

border observed in germline Myo5b KO mice, since Myo5b KO; Pacsin 2 KO mice showed similar loss of apical SGLT1, AQP7, and DPPIV (Fig. S4). These data demonstrate that inclusion formation is likely not the primary cause of mislocalization of apical membrane proteins that are responsible for sodium and water absorption in the small intestine in Myo5b KO mice (Engevik et al., 2018).

Discussion

Analysis of proximal small-intestinal explants and enteroids from Myo5b KO mice demonstrated that inclusions form from endocytosis of the apical membrane. The robust uptake of 70-kD FITC-dextran demonstrates that internalization of the brush border to form inclusions occurs through endocytosis in the neonatal intestine following loss of Myo5b. The presence of this endocytic process that is apparent after mutation of Myo5b is supported by a similar experiment performed in zebrafish goosepimple/Myo5b morpholinos that demonstrates uptake of Alexa Fluor 546–conjugated dextran in peridermal cells (Sonal et al., 2014). In Myo5b morphants, dextran-positive vesicles were enriched at the apical domain of peridermal cells, demonstrating that loss of Myo5b resulted in apical endocytosis (Sonal et al., 2014). Another report investigating loss of Myo5b in zebrafish showed the presence of numerous inclusions in the proximal midgut that were in close proximity to or contiguous with the apical membrane (Sidhaye et al., 2016). In addition to these zebrafish studies, our laboratory reported the presence of maternal murine IgG inside of inclusions in Myo5b KO enterocytes (Weis et al., 2016). Maternal IgG was surrounded by ezrin in Myo5b KO duodenal enterocytes, demonstrating that these inclusions originated from the apical brush border (Weis et al., 2016). Furthermore, organ culture of duodenal biopsies derived from individuals with MVID demonstrated that ovalbumin and

https://doi.org/10.1083/jcb.201902063

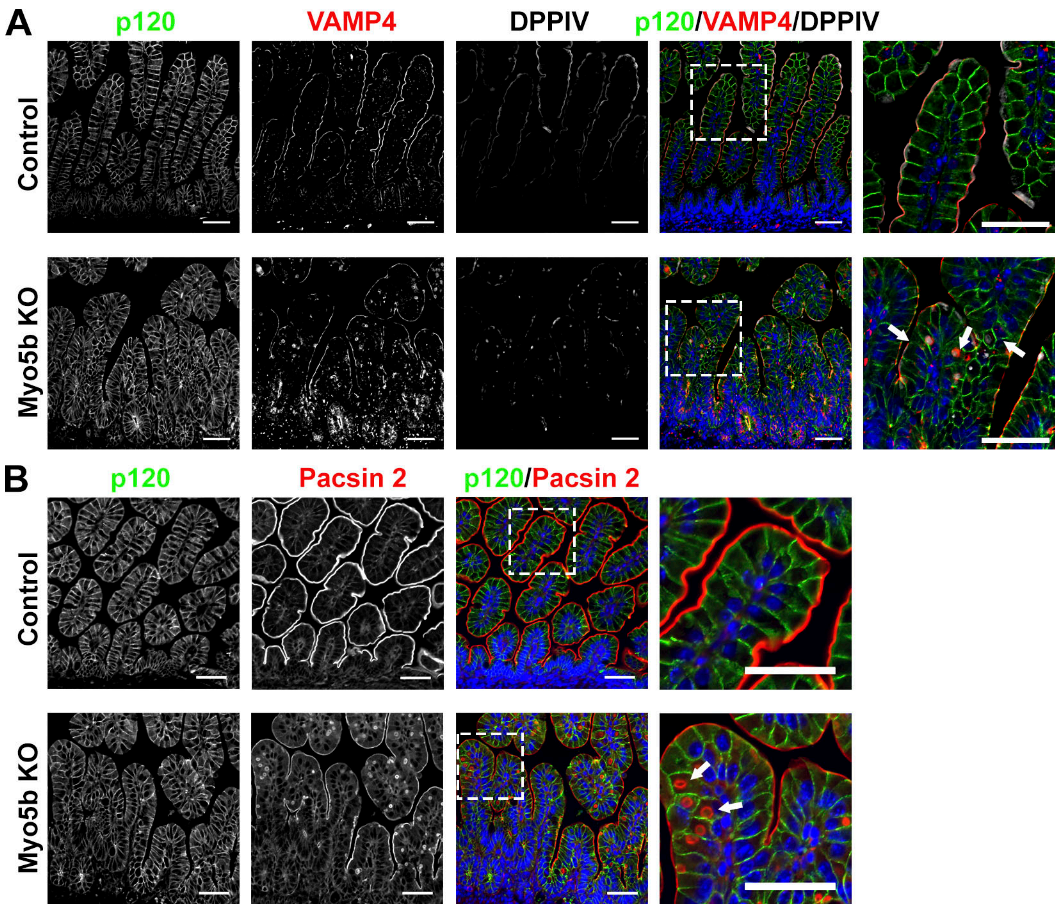

Figure 7. **Loss of Myo5b results in apical bulk endocytosis a pathway that shares characteristics with neuronal activity–dependent bulk endocytosis. (A)** VAMP4 (red), an essential cargo protein during ADBE, is present in the brush border of neonatal control enterocytes. In Myo5b KO mice, VAMP4 is still present on the apical membrane; however, numerous intracellular inclusions are positive for VAMP4. Many VAMP4-positive inclusions were double-positive for DPPIV (white) in Myo5b KO enterocytes. **(B)** The F-bar protein Pacsin 2 (red) was also observed on the apical membrane of control enterocytes. In Myo5b KO enterocytes, Pacsin 2 was expressed on the apical membrane and surrounding inclusions. *n* = 6 mice per group. Scale bars = 50 µm.

cationic-ferritin are endocytosed from the apical surface of enterocytes (Reinshagen et al., 2002). These data support the hypothesis that inclusions form through invaginations of the apical membrane following loss of Myo5b.

The large size of inclusions in Myo5b KO enterocytes and the uptake of 70-kD FITC-dextran suggested that inclusions might be forming through macropinocytosis. Macropinocytosis is a form of membrane internalization that is characterized by membrane ruffling to form large vesicles containing solute molecules, antigens, and nutrients (Lim and Gleeson, 2011). However, many of the characteristics of inclusion formation in Myo5b KO enterocytes suggest a distinct mechanism, one that more closely mirrors ADBE observed in hyperstimulated neurons. Unlike macropinocytosis, inclusions appear to form through invagination of the apical membrane and require excision from the brush border. EIPA treatment had no effect on inclusion formation in Myo5b KO–derived enteroids, supporting the conclusion that inclusions are not forming through macropinocytosis. Moreover, the association of Dynamin 2 with inclusions that are fully internalized and the accumulation of Dynamin 2 at the neck of inclusions that are still fused to the apical membrane suggest that Dynamin 2 is involved in the internalization and excision of inclusions. Previous reports have noted that macropinocytosis is independent of Dynamin 2 (Damke et al., 1995; Saeed et al., 2010; Devadas et al., 2014; Basagiannis et al., 2016). Our data support a dynamin-dependent endocytic mechanism given the increased number of inclusions present on the membrane of Myo5b KO enteroids and explants following inhibition of dynamin with Dyngo treatment. These findings indicate that dynamin is necessary for inclusion excision from the membrane through a mechanism that is distinct from macropinocytosis. We propose that the involvement of Pacsin 2 and Dynamin 2 represents a bulk endocytic process that is distinct from macropinocytosis and results in the internalization of the apical brush border to form large inclusions in Myo5b KO enterocytes.

Pacsins (syndapins) serve as molecular links between membrane trafficking and cortical cytoskeleton dynamics (Qualmann et al., 1999; Kessels and Qualmann, 2004). Our work indicates that microvillus inclusions originate from endocytosis and are dependent on dynamin and Pacsin 2. Interestingly, there is a single report in *C. elegans* intestine that Syndapin 1 is required for endocytic recycling (Gleason et al., 2016). This report demonstrated that Syndapin 1 was present in early and basolateral

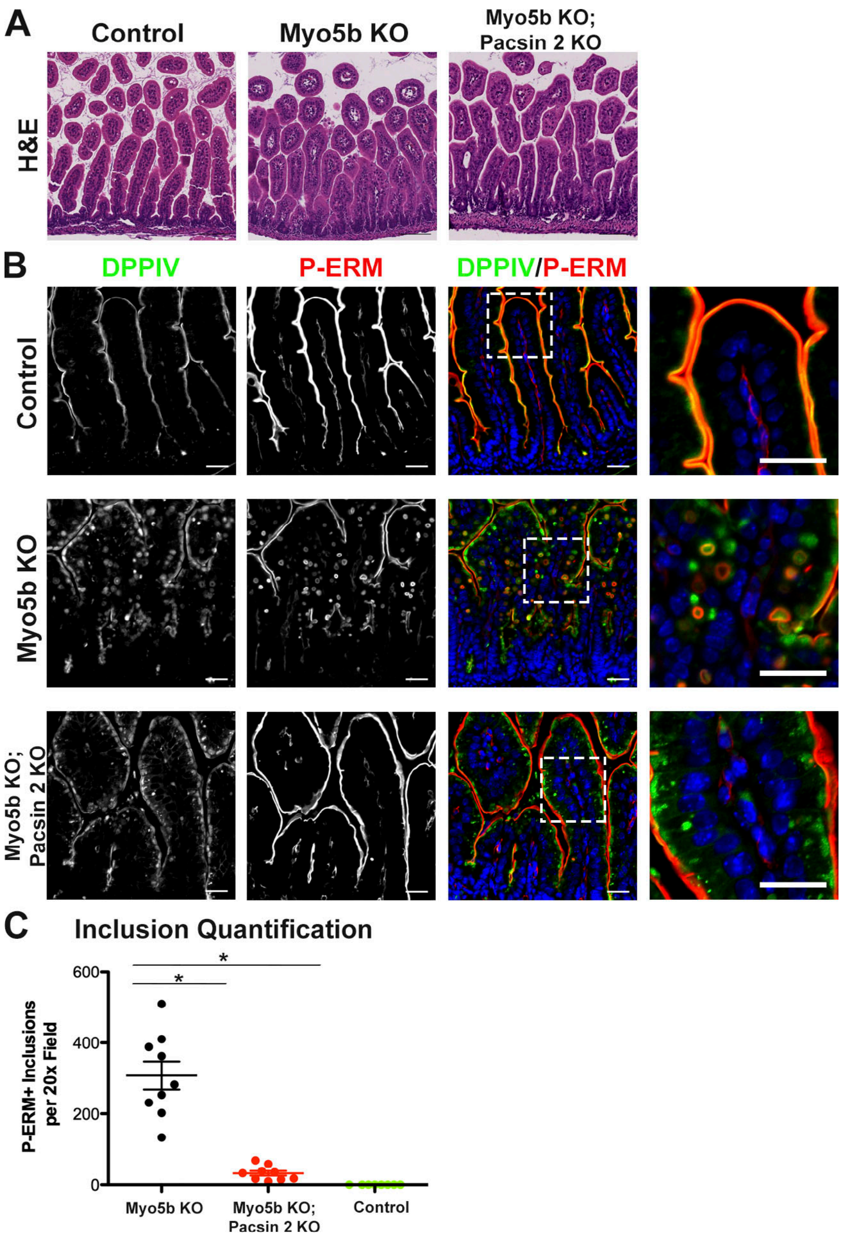

Figure 8. **Inclusion formation in Myo5b KO mice is dependent on Pacsin 2. (A)** H&E micrographs of the duodenum of control, Myo5b KO, and Myo5b KO mice crossed with Pacsin 2 KO mice (double KO mice, Myo5b KO;Pacsin 2 KO). **(B)** Crossing of Pacsin 2 KO mice with Myo5b KO mice to achieve a double KO of Myo5b and Pacsin 2 resulted in a significant decrease in P-ERM–positive (red) inclusions, suggesting that Pacsin 2 is required for inclusion formation. Despite decreased inclusion formation in Myo5b KO;Pacsin 2 KO (double KO) mice, DDPIV (green) was still mislocalized. **(C)** Inclusions, as defined by subapical P-ERM immunostaining, in three 20× fields were quantified per mouse to determine the impact of loss of Pacsin 2 on inclusion formation. Quantification of inclusions in the proximal small intestine (duodenum) demonstrated that Myo5b KO;Pacsin 2 KO (double KO) mice had significantly fewer inclusions than Myo5b KO mice, suggesting a critical role for Pacsin 2 in inclusion formation. n = 3 mice per group. Scale bars = 50 µm. One-way ANOVA was performed with the Bonferroni post hoc test for C; error bars are SEM. *, $P < 0.05$ compared to Myo5b KO mice.

recycling endosomes in the intestinal epithelium of *C. elegans*. Moreover, Syndapin 1 deletion mutants exhibited decreased basolateral recycling transport and accumulation of endosomes positive for early endosome and recycling endosome markers (Gleason et al., 2016). In mammals, the Pacsin 2 protein is primarily implicated in endocytosis, as it associates with multiple endocytic regulators including MICAL-L1, EHD1/mRme-1, and dynamin (Braun et al., 2005; Giridharan et al., 2013). Of note, *C. elegans* lack a MICAL-L1 homologue, which makes the worm model more reliant on Syndapin 1 for endocytic cargo recycling. Our work demonstrates the requirement for Pacsin 2 in inclusion formation in Myo5b KO mouse enterocytes, indicating that in mammals, Pacsin 2 may be more relevant to endocytosis in the intestinal epithelium.

We also report that inclusions are dependent on dynamin for scission from the apical membrane in Myo5b KO tissue and enteroids. These findings mirror those observed in ADBE in hyperstimulated neurons. Both apical bulk endocytosis in Myo5b KO enterocytes and ADBE in neurons have VAMP4 as a cargo (Nicholson-Fish et al., 2016), require dynamin, and involve Pacsin (syndapin; Clayton and Cousin, 2009). In the brain, inhibition of the Dynamin 1–sydnapin 1 interaction inhibits ADBE (Clayton et al., 2009). Similar to our studies, Clayton et al. (2009) demonstrated that inhibition of dynamin GTPase with the dynamin antagonist, Dynasore, resulted in reduction of high molecular weight dextran uptake by synaptic vesicles during intense neuronal stimulation. Additionally, administration of the calcineurin inhibitor cyclosporin A to enteroids resulted in a significant decrease in the total number of inclusions. Calcineurin regulates the retrieval of synaptic vesicles through ADBE (Evans and Cousin, 2007; Clayton and Cousin, 2008; Clayton et al., 2009). Cheung and Cousin (2013) demonstrated that inhibition of the calcium-dependent protein phosphatase calcineurin prevented endosomal synaptic vesicle formation, which closely corresponds to our findings in neonatal enterocytes. In the intestine of neonatal Myo5b KO mice, inclusion formation is dependent on Pacsin 2, since mice lacking both Myo5b and Pacsin 2 had significantly fewer inclusions than Myo5b KO mice. Similarly, knockdown of Syndapin 1 with shRNA disrupted ADBE in neuronal cultures (Clayton et al., 2009). Moreover, overexpression of dominant-negative Dynamin 1 mutants that are unable to interact with syndapin prevents ADBE (Anggono et al., 2006). Additionally, presynaptic microinjection of syndapin antibodies or Fab fragments into lamprey reticulospinal tract results in arrest of ADBE (Andersson et al., 2008). All of these findings support the similarity of apical bulk endocytosis in Myo5b enterocytes to ADBE in hyperstimulated neurons.

We demonstrated that fewer inclusions did not ameliorate the intestinal phenotype of loss of Myo5b, supporting the concept that inclusion formation is not a primary cause of the pathological mislocalization of transporters observed in the intestine following loss of Myo5b. Mice lacking both Myo5b and Pacsin 2 had altered expression of key apical membrane transporters (AQP7 and SGLT1) that facilitate water absorption. Moreover, Myo5b;Pacsin 2 double KO mice died shortly after birth, similar to Myo5b KO mice. The early demise of Myo5b;Pacsin 2 double KO mice suggests that loss of Myo5b likely disrupts the delivery of proteins to the apical brush border. We propose that this pathway is independent of apical bulk endocytosis, which is supported by our findings in Myo5b;Pacsin 2 double KO mice. Moreover, induction of Myo5b loss in adult VilCre^{ERT2};Myo5b$^{fl/fl}$ mice resulted in few inclusions; however, VilCre^{ERT2};Myo5b$^{fl/fl}$ mice still exhibited alterations in proteins normally expressed at the apical membrane (Weis et al., 2016; Engevik et al., 2018). These results suggest that adult VilCre^{ERT2};Myo5b$^{fl/fl}$ mice display a defect in delivery of apical brush border proteins that does not result from apical bulk endocytosis.

While our data demonstrate that inclusions are formed through apical bulk endocytosis, it is less clear how this process is initiated. Loss of Myo5b should alter vesicle trafficking by a number of Rab proteins including Rab11a, Rab11b, Rab25, and Rab8a, and Myo5b KO enterocytes also show a loss of subapical activated cdc42 (Knowles et al., 2014; Weis et al., 2016). Induction of Myo5b KO with tamoxifen treatment in VilCre^{ERT2};Myo5b$^{fl/fl}$ mice induces formation of microvillus inclusions in enterocytes emerging from intestinal crypts, with inclusion formation more evident in induced neonates compared with adults (Weis et al., 2016). Thus, loss of Myo5b may directly activate this endocytic mechanism. Alternatively, loss of Myo5b may alter trafficking patterns, leading to exaggeration of this pathway. The fragmentation of the giant lysosomes usually found in neonatal enterocytes suggests that processing of membranes into lysosomes may be impaired following Myo5b loss (Schneeberger et al., 2015; Weis et al., 2016; Engevik et al., 2018). Microvillus-lined inclusions in Myo5b KO mice were associated with membrane tubules containing the apical endosomal protein, endotubin, which is highly expressed in intestinal epithelium before weaning. However, in adulthood, endotubin decreases to approximately half of the levels observed in neonatal enterocytes (Wilson et al., 1991; Cox et al., 2017). Endotubin is an integral membrane protein concentrated in the tubular apical endosome and is thought to be a scaffold regulating apical membrane trafficking (Wilson et al., 1987, 1991; Cox et al., 2017). Thus, endotubin likely plays a critical role in endocytosis early in development. In a recent publication, Cox et al. (2017) demonstrated that loss of endotubin resulted in disruption of the apical endocytic complex and formation of inclusions in mice early in life before weaning. Similarly, neonatal Myo5b KO mice showed large intracellular inclusions, many of which were ringed by endotubin. Nascent inclusions forming at the apical membrane, in particular, were surrounded by endotubin.

During early life, the apical endocytic complex plays a critical role in the uptake of luminal contents and sorting of growth factors (Gonnella and Neutra, 1984, 1985; Siminoski et al., 1986; Gonnella et al., 1987). Previous studies have suggested that, in humans, maternal IgG is taken up from maternal milk through facilitated clathrin-dependent endocytosis of IgG bound to the neonatal Fc receptor. However, neonatal small-intestinal enterocytes are highly endocytic, with well-developed tubular apical endosomal complexes (Wissig and Graney, 1968; Knutton et al., 1974; Gonnella and Neutra, 1984; Wilson et al., 1987, 1991; Arévalo Sureda et al., 2016; Cox et al., 2017). This endosomal system, which is defined by the expression of endotubin, is thought to process apical luminal contents during the first days of life. Uptake of large quantities of luminal nutrition may also facilitate the transfer of nerve growth factor and epidermal growth factor into the circulation (Gonnella and Neutra, 1984; Siminoski et al., 1986; Gonnella et al., 1987; Kumagai et al., 2011). Absorption of high concentrations of vitamins has also been documented (Goncalves et al., 2014, 2015), suggesting that this endocytic process could provide an important pathway for the uptake of luminal contents during early life. Since inclusion formation is most prevalent in neonatal Myo5b KO mice (Weis et al., 2016), it is possible that loss of Myo5b results in a perturbation of endosome processing through the endotubin-containing sorting system into lysosomes.

Collectively, the data indicate that loss of Myo5b induces an apical bulk endocytic pathway in small-intestinal enterocytes. In both tissue explants and enteroids from Myo5b KO mice, we have only identified evidence for apical bulk endocytosis. We have also defined apical bulk endocytosis in Myo5b KO enterocytes as a pathway with characteristics overlapping with neuronal ADBE. We postulate that, similar to ADBE, the use of apical bulk endocytosis in the neonatal enterocytes may provide a rapid membrane uptake mechanism adapted for the needs of gut function early in life. With loss of Myo5b, this pathway may be perturbed due to the blockade of trafficking that results from mutations in Myo5b.

Materials and methods

Animals

The Institutional Animal Care and Use Committee of Vanderbilt University Medical Center approved all experimental procedures and animal care and maintenance. Germline Myo5b KO mice were generated as previously reported (Weis et al., 2016). Mice heterozygous for Myo5b KO were crossed with LifeAct mice to generate Myo5b KO;LifeAct mice to visualize F-actin (Engevik et al., 2018). Mice heterozygous for Myo5b KO were crossed with Pacsin 2 KO mice to generate double KO mice that lack both Myo5b and Pacsin 2. The proximal small intestine (duodenum and jejunum) of mice 1–5 d old (neonatal) were used for all experiments. Control mice were littermates whenever possible and were either heterozygous or WT for Myo5b. The intestines were excised and fixed in 4% PFA in PBS (Thermo Fisher Scientific, J19943) or 10% neutral buffered formalin (VWR, 16004-128) overnight at 4°C and embedded in paraffin. Different fixations were used for optimal antibody staining. For frozen embedded tissue, intestine was fixed in 4% PFA for 1 h at room temperature, washed once in PBS for 5 min, and then embedded in optimal cutting temperature compound (Sakura, 4583) and frozen on dry ice. Frozen sections were cut at a thickness of 5 µm using a cryostat and were used for staining.

Immunofluorescence

Paraffin-embedded slides

Slides were warmed on a heating block for 15 min before deparaffinization in Histoclear (National Diagnostics, HS-200). Sections were rehydrated, and antigen retrieval was performed in 1× citrate buffer, pH 6.0 (Dako, S1699), in a pressure cooker for 15 min on high-pressure setting. Slides were cooled on ice and then blocked for 1.5 h with serum-free protein block (Dako, X0909). For mouse antibodies, an additional mouse-on-mouse block (Vector Laboratories, MKB-2213) was used for 20 min at room temperature followed by a PBS wash. Primary antibodies were then incubated overnight at 4°C. Three washes with PBS were performed, and sections were incubated for 1 h at room temperature with secondary antibodies. 1:1,000 Hoechst (Thermo Fisher Scientific, 62249; 10 mg/ml) was added to each section, followed by three washes in PBS. One drop of ProLong Gold antifade reagent was added to slides to coverslip (Thermo Fisher Scientific, P36934).

Microscope image acquisition

All slides were analyzed using a Zeiss Axio Imager.M2 microscope equipped with an Axiovision digital imaging system (Zeiss) using 20× or 40× objectives or a Zeiss LSM 880 Axio observer confocal microscope with Airyscan using a 63× objective (Zeiss). The 20× objective for the Axio imager was a Plan-apochromat with a numerical aperture of 0.8 M27. The 40× objective for the Axio imager was a Plan-apochromat with a numerical aperture of 0.95 Korr M27. The 63× objective for the Zeiss LSM 880 confocal microscope was a Plan-apochromat oil-immersion objective for Airyscan with a numerical aperture of 1.4. Fluorescent donkey secondary antibodies were used that were conjugated to Alexa Fluor 488, Cy3, Cy5, or Alexa Fluor 796. Imaging of fixed tissue was performed at room temperature; all specimens were mounted in ProLong Gold antifade reagent before imaging. The camera used to acquire images on the Axio Imager microscope was the AxioCam HRm Rev.3. For images acquired using the Zeiss LSM 880 Airyscan, superresolution processing was used. Axiovision digital imaging system and Zen blue software were used to export single-channel tiff images for all images acquired. Adobe Photoshop was used to merge images.

Frozen slides

Frozen sections were equilibrated and washed in PBS for 10 min. Sections were permeabilized with 0.1% Triton X-100 in PBS for 30 min and then blocked with 10% normal donkey serum for 30 min. Primary antibody was applied in 0.05% Tween 20 and 1% normal donkey serum and incubated overnight at 4°C. Slides were washed three times in PBS for 5 min each and incubated with appropriate secondary antibodies for 1 h at room temperature. Hoechst was used to stain nuclei, and slides were washed with PBS three times. Sections were coverslipped using ProLong Gold (Thermo Fisher Scientific, P36934) and imaged.

Primary antibodies

The following primary antibodies and dilutions were used for immunostaining: P-ERM rabbit 1:200 (Cell Signaling, 3726S), DPPIV goat 1:200 (R&D Systems, AF954), Pacsin 2 rabbit (Syndapin 2) 1:100 (Sigma-Aldrich, HPA-049854), Dynamin 2 rabbit 1:200 (Novus, NBP2-47477), VAMP4 rabbit 1:200 (Synaptic Systems, 136 002), p120 mouse 1:200 (BD Biosciences, 610133), and Endotubin mouse 1:1 (Wilson et al., 1987).

Dextran uptake in explants mounted in Üssing chambers

The proximal half of the small intestine (duodenum and jejunum) was opened along the mesenteric border, and luminal contents were gently removed under a stereomicroscope in ice-cold Krebs-Ringer buffer. Whole-thickness mucosal sheets (two to six explants per mouse) were mounted in sliders with an aperture of 0.031 cm^2 (Physiological Instruments). Luminal and serosal surfaces of tissue were bathed with 4 ml Krebs-Ringer buffer, bubbled with a gas mixture of 95% O_2-5% CO_2 to maintain the pH at 7.4, and maintained at 37°C. The bathing solution contained 117 mM NaCl, 4.7 mM KCl, 1.2 mM $MgCl_2$, 2.5 mM $CaCl_2$, 1.2 mM NaH_2PO_4, 25 mM $NaHCO_3$, 11 mM glucose, and GlutaMax (Thermo Fisher Scientific, 35050-061). To prevent prostaglandin synthesis, the cyclooxygenase inhibitor, indomethacin (10 µM), was added to the serosal bath. After a 15-min stabilization period, 20 µg/ml of FITC-conjugated dextran (70 kD) solution was applied into the luminal bath in the presence or absence of inhibitors and incubated for 4 h. After incubation, the tissue was fixed in 4% PFA for 1 h at room temperature and then washed for 5 min in PBS five times. Intestinal explants were frozen in optimal cutting temperature compound, and 5-µm sections were cut. Alexa Fluor 568–conjugated phalloidin (1:100 in PBS; Thermo Fisher Scientific, A12380) was used to label F-actin for 1 h at room temperature. Hoechst was added to identify nuclei, followed by three washes in PBS. Samples were then coverslipped and imaged to determine FITC dextran uptake.

Enteroid culture

Enteroids were generated from neonatal Myo5b KO and control mice following a previously published protocol (Mahe et al., 2013). Briefly, crypts were isolated from the proximal small intestine of neonatal mice by incubating small pieces of tissue in 2 mM EDTA in PBS for 30 min at 4°C. The EDTA solution was then removed, and 55 mM D-sorbitol and 34 mM sucrose (in PBS) solution was added to the tissue. The tubes were shaken vigorously for 1 min. Supernatant was inspected to determine quality and quantity of dissociated crypts. The shaken solution containing tissue and crypts was strained through a 70-µm strainer (Corning, 431751), and the flow-through was centrifuged at 300 *g* for 5 min. The resulting pellet was resuspended in Matrigel (Corning, 356231) and distributed as domes in a 48-well plate that was incubated at 37°C for 15 min to allow the Matrigel to polymerize. Crypt suspensions in Matrigel were overlaid with prewarmed mouse Intesticult media (Stem Cell Technologies, 06000). Enteroids were differentiated before analysis by withdrawal of Wnt. For immunostaining, enteroids were fixed for 30 min at room temperature with 4% PFA. Enteroids were washed with PBS for 5 min and then embedded in Histogel (Thermo Fisher Scientific, HG-4000-012) for paraffin embedding, or whole-mount immunofluorescence was performed. Enteroids were treated for 4 h with 30 µM Dyngo (Abcam, ab120689), 20 µM cyclosporin (Sigma-Aldrich, 30024), 30 µM EIPA (Sigma-Aldrich, A3085) or vehicle (DMSO; Sigma-Aldrich, D2650) to determine whether compounds influenced inclusion formation.

Live-cell imaging

Live-cell imaging of LifeAct control and LifeAct;Myo5b KO enteroids was performed using a Nikon Ti2 inverted light microscope with a Yokogawa CSU-X1 spinning disk head. An Andor DU-897 EMCCD camera was used to acquire images. Overnight imaging (~16 h) was performed at 37°C with 5% CO_2 using a Plan Apo λ 20× objective with a numerical aperture of 0.75. 0.5-µm sections were acquired every 2 min. Enteroids were imaged in differentiation media while embedded in Matrigel. A 488-nm emission laser was used to visualize LifeAct-GFP. Nikon Elements software was used for acquisition and image processing.

TEM

Differentiated enteroids were washed in 0.1 mol/liter cacodylate buffer and then fixed in 2.5% glutaraldehyde for 1 h at room temperature. Enteroids were stored at 4°C before processing. Briefly, on a rotating wheel, the fixed samples were washed in 0.1 mol/liter cacodylate buffer, and then incubated for 1 h at room temperature in 1% osmium tetroxide. After washing again with cacodylate buffer followed by a brief water wash, the samples were stained en bloc with 2% ethanolic uranyl acetate for 30 min at room temperature in the dark. After en bloc staining, the samples were rinsed with water and dehydrated through an ethanol series (30, 50, 75, 85, and 95%) and three changes of 100% ethanol for 15 min each. The samples were further dehydrated with propylene oxide followed by resin infiltration (Embed 812; EMS). Samples were infiltrated in a 2:1 mixture of propylene oxide and resin for 30 min, then 1:1 for 1 h and then overnight. The next day, the samples were incubated in a 1:2 mixture of propylene oxide and resin for 3 h. The samples were further infiltrated with pure resin for another 24–36 h and then embedded and polymerized for 48 h at 60°C. 1-µm-thick sections were cut and stained with toluidine blue to identify the region of interest for thin sectioning. Once identified, 70-nm thin sections were collected on copper grids and post-stained with 2% uranyl acetate and Reynold's lead citrate. Samples were subsequently imaged, at various magnifications, on the Philips/FEI Tecnai 12 (T12) transmission electron microscope. Imaging was performed at the Vanderbilt Imaging Core.

Quantification of inclusions in paraffin-embedded tissue and intestinal explants

For quantification of inclusions in paraffin-embedded sections (P-ERM, Endotubin, VAMP4, and Pacsin 2), three fields at 20× of the proximal duodenum were analyzed in at least three mice per group. Regions were chosen based on location, quality of staining, and tissue architecture, allowing for complete visualization of villi and quantification of inclusions. Similar regions of the proximal small intestine were imaged between control and Myo5b KO mice and Myo5b KO;Pacsin 2 KO mice. All inclusions in a 20× field were quantified based on staining for brush border components of interest, which included Endotubin, P-ERM, VAMP4, and Pacsin 2. Explant experiments in Üssing chambers were performed with five control mice and five Myo5b KO mice to determine the mechanism of FITC-dextran uptake into inclusions. DMSO treatment was performed on five Myo5b KO mice, while Dyngo treatment was performed on four Myo5b KO mice. For each explant experiment, two to six explants were mounted per mouse to provide at least biological duplicates. For quantification of explant experiments, images were acquired using a 40× objective on a Zeiss Axiovision digital imaging system, and the whole section of each individual explant (~0.05 cm^2) was analyzed for number of F-actin–positive inclusions and number of inclusions containing FITC-dextran. To better examine the presence of FITC-dextran in inclusions, images were taken on a Zeiss LSM 880 microscope using a 63× objective. To determine whether administration of Dyngo prevented fission of inclusions from the apical membrane, the entire explant was imaged, and the total number of inclusions that were attached to the apical membrane and fully internalized was quantified, and the percentage of inclusions remaining at the apical membrane was calculated. For quantification of FITC-dextran internalization in Myo5b KO explants treated with DMSO or Dyngo, the number of FITC-dextran and F-actin double-positive inclusions was counted, and the number of total F-actin inclusions was quantified. The percentage of inclusions containing FITC-dextran was calculated. Each explant from four to five mice is represented in Fig. 6 C.

Statistical analysis

Comparisons between genotypes and treatment groups were made using Student's *t* test (one-sided) or one-way ANOVA, and the Bonferroni post hoc test was used to determine significance using Prism software (GraphPad Software). Data distribution was assumed to be normal but was not formally tested. A P value <0.05 was considered significant for all experiments. Error bars are SEM.

Online supplemental material

Fig. S1 shows live imaging of control LifeAct-derived enteroids demonstrating no internalization of F-actin. Fig. S2 shows control enteroids treated with DMSO, Dyngo, EIPA, and cyclosporin, demonstrating no alterations in apical membrane. Fig. S3 shows quantification of inclusions containing endotubin, P-ERM, VAMP4, or Pacsin 2 in Myo5B KO mouse intestine. Fig. S4 demonstrates that decreased inclusion formation does not correlate with improved trafficking of apical membrane proteins. Video 1 displays live imaging confocal microscopy of enteroids expressing LifeAct derived from the proximal small intestine of control mice. Video 2 displays inclusion formation in LifeAct;Myo5b KO enteroids using confocal microscopy.

Acknowledgments

This work was supported by National Institutes of Health grants R01 DK48370 and R01 DK70856 and a gift from the Christine Volpe Fund to J.R. Goldenring. A.C. Engevik was supported by National Institutes of Health grant F32 DK111101. M.J. Tyska was supported by National Institutes of Health grants R01 DK111949 and R01 DK095811. J.M. Wilson was supported by National Institutes of Health grant 1R01 DK109701. This work was supported by core resources of the Vanderbilt Digestive Disease Center (P30 DK058404) and the Vanderbilt-Ingram Cancer Center (P30 CA68485), and imaging was supported by both the Vanderbilt Cell Imaging Shared Resource and the Vanderbilt Digital Histology Shared Resource (supported by a U.S. Department of Veterans Affairs Shared Equipment Grant, 1IS1BX003097).

The authors declare no competing financial interests.

Author contributions: A.C. Engevik, I. Kaji, A.R. Meyer, and G.N. Fitz performed the mouse tissue studies and staining. A.C. Engevik developed the mouse organoids and performed imaging studies on organoids. A.C. Engevik, M.M. Postema, and J.J. Faust performed live-cell imaging studies in enteroids. J.A. Williams performed EM studies with A.C. Engevik. M.J. Tyska, J.M. Wilson, and J.R. Goldenring participated in experimental design and data analysis. A.C. Engevik wrote the initial draft of the manuscript and coordinated revisions in consultation with J.R. Goldenring and all of the other authors.

Submitted: 11 February 2019
Revised: 22 May 2019
Accepted: 29 August 2019

References

Andersson, F., J. Jakobsson, P. Löw, O. Shupliakov, and L. Brodin. 2008. Perturbation of syndapin/PACSIN impairs synaptic vesicle recycling evoked by intense stimulation. *J. Neurosci.* 28:3925–3933. https://doi.org/10.1523/JNEUROSCI.1754-07.2008

Anggono, V., K.J. Smillie, M.E. Graham, V.A. Valova, M.A. Cousin, and P.J. Robinson. 2006. Syndapin I is the phosphorylation-regulated dynamin I partner in synaptic vesicle endocytosis. *Nat. Neurosci.* 9:752–760. https://doi.org/10.1038/nn1695

Arévalo Sureda, E., B. Weström, S.G. Pierzynowski, and O. Prykhodko. 2016. Maturation of the Intestinal Epithelial Barrier in Neonatal Rats Coincides with Decreased FcRn Expression, Replacement of Vacuolated Enterocytes and Changed Blimp-1 Expression. *PLoS One.* 11:e0164775. https://doi.org/10.1371/journal.pone.0164775

Azzi, J.R., M.H. Sayegh, and S.G. Mallat. 2013. Calcineurin inhibitors: 40 years later, can't live without... *J. Immunol.* 191:5785–5791. https://doi.org/10.4049/jimmunol.1390055

Basagiannis, D., S. Zografou, C. Murphy, T. Fotsis, L. Morbidelli, M. Ziche, C. Bleck, J. Mercer, and S. Christoforidis. 2016. VEGF induces signalling and angiogenesis by directing VEGFR2 internalisation through macropinocytosis. *J. Cell Sci.* 129:4091–4104.

Bidaud-Meynard, A., O. Nicolle, M. Heck, Y. Le Cunff, and G. Michaux. 2019. A V0-ATPase-dependent apical trafficking pathway maintains the polarity of the intestinal absorptive membrane. *Development.* 146: dev174508. https://doi.org/10.1242/dev.174508

Braun, A., R. Pinyol, R. Dahlhaus, D. Koch, P. Fonarev, B.D. Grant, M.M. Kessels, and B. Qualmann. 2005. EHD proteins associate with syndapin I and II and such interactions play a crucial role in endosomal recycling. *Mol. Biol. Cell.* 16:3642–3658. https://doi.org/10.1091/mbc.e05-01-0076

Cartón-García, F., A.W. Overeem, R. Nieto, S. Bazzocco, H. Dopeso, I. Macaya, J. Bilic, S. Landolfi, J. Hernandez-Losa, S. Schwartz Jr., et al. 2015. Myo5b knockout mice as a model of microvillus inclusion disease. *Sci. Rep.* 5:12312. https://doi.org/10.1038/srep12312

Cheung, G., and M.A. Cousin. 2013. Synaptic vesicle generation from activity-dependent bulk endosomes requires calcium and calcineurin. *J. Neurosci.* 33:3370–3379. https://doi.org/10.1523/JNEUROSCI.4697-12.2013

Cheung, G., O.J. Jupp, and M.A. Cousin. 2010. Activity-dependent bulk endocytosis and clathrin-dependent endocytosis replenish specific synaptic vesicle pools in central nerve terminals. *J. Neurosci.* 30:8151–8161. https://doi.org/10.1523/JNEUROSCI.0293-10.2010

Clayton, E.L., and M.A. Cousin. 2008. Differential labelling of bulk endocytosis in nerve terminals by FM dyes. *Neurochem. Int.* 53:51–55. https://doi.org/10.1016/j.neuint.2008.06.002

Clayton, E.L., and M.A. Cousin. 2009. The molecular physiology of activity-dependent bulk endocytosis of synaptic vesicles. *J. Neurochem.* 111: 901–914. https://doi.org/10.1111/j.1471-4159.2009.06384.x

Clayton, E.L., G.J. Evans, and M.A. Cousin. 2008. Bulk synaptic vesicle endocytosis is rapidly triggered during strong stimulation. *J. Neurosci.* 28: 6627–6632. https://doi.org/10.1523/JNEUROSCI.1445-08.2008

Clayton, E.L., V. Anggono, K.J. Smillie, N. Chau, P.J. Robinson, and M.A. Cousin. 2009. The phospho-dependent dynamin-syndapin interaction triggers activity-dependent bulk endocytosis of synaptic vesicles. *J. Neurosci.* 29:7706–7717. https://doi.org/10.1523/JNEUROSCI.1976-09.2009

Commisso, C., S.M. Davidson, R.G. Soydaner-Azeloglu, S.J. Parker, J.J. Kamphorst, S. Hackett, E. Grabocka, M. Nofal, J.A. Drebin, C.B. Thompson, et al. 2013. Macropinocytosis of protein is an amino acid supply route in Ras-transformed cells. *Nature.* 497:633–637. https://doi.org/10.1038/nature12138

Côte, M., M.M. Ménager, A. Burgess, N. Mahlaoui, C. Picard, C. Schaffner, F. Al-Manjomi, M. Al-Harbi, A. Alangari, F. Le Deist, et al. 2009. Munc18-2 deficiency causes familial hemophagocytic lymphohistiocytosis type 5 and impairs cytotoxic granule exocytosis in patient NK cells. *J. Clin. Invest.* 119:3765–3773. https://doi.org/10.1172/JCI40732

Cox, C.M., R. Lu, K. Salcin, and J.M. Wilson. 2017. The Endosomal Protein Endotubin Is Required for Enterocyte Differentiation. *Cell. Mol. Gastroenterol. Hepatol.* 5:145–156. https://doi.org/10.1016/j.jcmgh.2017.11.001

Cutz, E., J.M. Rhoads, B. Drumm, P.M. Sherman, P.R. Durie, and G.G. Forstner. 1989. Microvillus inclusion disease: an inherited defect of brush-border assembly and differentiation. *N. Engl. J. Med.* 320:646–651. https://doi.org/10.1056/NEJM198903093201006

Damke, H., T. Baba, A.M. van der Bliek, and S.L. Schmid. 1995. Clathrin-independent pinocytosis is induced in cells overexpressing a temperature-sensitive mutant of dynamin. *J. Cell Biol.* 131:69–80. https://doi.org/10.1083/jcb.131.1.69

Davidson, G.P., E. Cutz, J.R. Hamilton, and D.G. Gall. 1978. Familial enteropathy: a syndrome of protracted diarrhea from birth, failure to thrive, and hypoplastic villus atrophy. *Gastroenterology.* 75:783–790. https://doi.org/10.1016/0016-5085(78)90458-4

De Camilli, P., K. Takei, and P.S. McPherson. 1995. The function of dynamin in endocytosis. *Curr. Opin. Neurobiol.* 5:559–565. https://doi.org/10.1016/0959-4388(95)80059-X

Devadas, D., T. Koithan, R. Diestel, U. Prank, B. Sodeik, and K. Döhner. 2014. Herpes simplex virus internalization into epithelial cells requires Na+/H+ exchangers and p21-activated kinases but neither clathrin- nor caveolin-mediated endocytosis. *J. Virol.* 88:13378–13395. https://doi.org/10.1128/JVI.03631-13

Dharmalingam, E., A. Haeckel, R. Pinyol, L. Schwintzer, D. Koch, M.M. Kessels, and B. Qualmann. 2009. F-BAR proteins of the syndapin family shape the plasma membrane and are crucial for neuromorphogenesis. *J. Neurosci.* 29:13315–13327. https://doi.org/10.1523/JNEUROSCI.3973-09.2009

Engevik, A.C., I. Kaji, M.A. Engevik, A.R. Meyer, V.G. Weis, A. Goldstein, M.W. Hess, T. Muller, H. Koepsell, P.K. Dudeja, et al. 2018. Loss of

MYO5B Leads to Reductions in Na(+) Absorption With Maintenance of CFTR-Dependent Cl(-) Secretion in Enterocytes. *Gastroenterology*. 155: 1883–1897.e10. https://doi.org/10.1053/j.gastro.2018.08.025

Erickson, R.P., K. Larson-Thomé, R.K. Valenzuela, S.E. Whitaker, and M.D. Shub. 2008. Navajo microvillous inclusion disease is due to a mutation in MYO5B. *Am. J. Med. Genet. A*. 146A:3117–3119. https://doi.org/10.1002/ajmg.a.32605

Evans, G.J., and M.A. Cousin. 2007. Activity-dependent control of slow synaptic vesicle endocytosis by cyclin-dependent kinase 5. *J. Neurosci.* 27: 401–411. https://doi.org/10.1523/JNEUROSCI.3809-06.2007

Giridharan, S.S., B. Cai, N. Vitale, N. Naslavsky, and S. Caplan. 2013. Cooperation of MICAL-L1, syndapin2, and phosphatidic acid in tubular recycling endosome biogenesis. *Mol. Biol. Cell.* 24:1776–1790. https://doi.org/10.1091/mbc.e13-01-0026

Gleason, A.M., K.C. Nguyen, D.H. Hall, and B.D. Grant. 2016. Syndapin/SDPN-1 is required for endocytic recycling and endosomal actin association in the C. elegans intestine. *Mol. Biol. Cell.* 27:3746–3756. https://doi.org/10.1091/mbc.e16-02-0116

Golachowska, M.R., C.M. van Dael, H. Keuning, A. Karrenbeld, D. Hoekstra, C.F. Gijsbers, M.A. Benninga, E.H. Rings, and S.C. van Ijzendoorn. 2012. MYO5B mutations in patients with microvillus inclusion disease presenting with transient renal Fanconi syndrome. *J. Pediatr. Gastroenterol. Nutr.* 54:491–498. https://doi.org/10.1097/MPG.0b013e3182353773

Goncalves, A., M. Margier, S. Roi, X. Collet, I. Niot, P. Goupy, C. Caris-Veyrat, and E. Reboul. 2014. Intestinal scavenger receptors are involved in vitamin K1 absorption. *J. Biol. Chem.* 289:30743–30752. https://doi.org/10.1074/jbc.M114.587659

Goncalves, A., S. Roi, M. Nowicki, A. Dhaussy, A. Huertas, M.J. Amiot, and E. Reboul. 2015. Fat-soluble vitamin intestinal absorption: absorption sites in the intestine and interactions for absorption. *Food Chem.* 172:155–160. https://doi.org/10.1016/j.foodchem.2014.09.021

Gonnella, P.A., and M.R. Neutra. 1984. Membrane-bound and fluid-phase macromolecules enter separate prelysosomal compartments in absorptive cells of suckling rat ileum. *J. Cell Biol.* 99:909–917. https://doi.org/10.1083/jcb.99.3.909

Gonnella, P.A., and M.R. Neutra. 1985. Glycoconjugate distribution and mobility on apical membranes of absorptive cells of suckling rat ileum in vivo. *Anat. Rec.* 213:520–528. https://doi.org/10.1002/ar.1092130408

Gonnella, P.A., K. Siminoski, R.A. Murphy, and M.R. Neutra. 1987. Transepithelial transport of epidermal growth factor by absorptive cells of suckling rat ileum. *J. Clin. Invest.* 80:22–32. https://doi.org/10.1172/JCI113051

Ivanov, A.I. 2008. Pharmacological inhibition of endocytic pathways: is it specific enough to be useful? *Methods Mol. Biol.* 440:15–33. https://doi.org/10.1007/978-1-59745-178-9_2

Kessels, M.M., and B. Qualmann. 2004. The syndapin protein family: linking membrane trafficking with the cytoskeleton. *J. Cell Sci.* 117:3077–3086. https://doi.org/10.1242/jcs.01290

Knowles, B.C., J.T. Roland, M. Krishnan, M.J. Tyska, L.A. Lapierre, P.S. Dickman, J.R. Goldenring, and M.D. Shub. 2014. Myosin Vb uncoupling from RAB8A and RAB11A elicits microvillus inclusion disease. *J. Clin. Invest.* 124:2947–2962. https://doi.org/10.1172/JCI71651

Knutton, S., A.R. Limbrick, and J.D. Robertson. 1974. Regular structures in membranes. I. Membranes in the endocytic complex of ileal epithelial cells. *J. Cell Biol.* 62:679–694. https://doi.org/10.1083/jcb.62.3.679

Koivusalo, M., C. Welch, H. Hayashi, C.C. Scott, M. Kim, T. Alexander, N. Touret, K.M. Hahn, and S. Grinstein. 2010. Amiloride inhibits macropinocytosis by lowering submembranous pH and preventing Rac1 and Cdc42 signaling. *J. Cell Biol.* 188:547–563. https://doi.org/10.1083/jcb.200908086

Kumagai, N., R. Baba, Y. Sakuma, K. Arita, M. Shinohara, M. Kourogi, S. Fujimoto, and M. Fujita. 2011. Origin of the apical transcytic membrane system in jejunal absorptive cells of neonates. *Med. Mol. Morphol.* 44: 71–78. https://doi.org/10.1007/s00795-010-0506-3

Li, L., T. Wan, M. Wan, B. Liu, R. Cheng, and R. Zhang. 2015. The effect of the size of fluorescent dextran on its endocytic pathway. *Cell Biol. Int.* 39: 531–539. https://doi.org/10.1002/cbin.10424

Lim, J.P., and P.A. Gleeson. 2011. Macropinocytosis: an endocytic pathway for internalising large gulps. *Immunol. Cell Biol.* 89:836–843. https://doi.org/10.1038/icb.2011.20

Mahe, M.M., E. Aihara, M.A. Schumacher, Y. Zavros, M.H. Montrose, M.A. Helmrath, T. Sato, and N.F. Shroyer. 2013. Establishment of Gastrointestinal Epithelial Organoids. *Curr. Protoc. Mouse Biol.* 3:217–240. https://doi.org/10.1002/9780470942390.mo130179

Mosa, M.H., O. Nicolle, S. Maschalidi, F.E. Sepulveda, A. Bidaud-Meynard, C. Menche, B.E. Michels, G. Michaux, G. De Saint Basile, and H.F. Farin. 2018. Dynamic Formation of Microvillus Inclusions During Enterocyte Differentiation in Munc18-2-Deficient Intestinal Organoids. *Cell. Mol. Gastroenterol. Hepatol.* 6:477–493.e1. https://doi.org/10.1016/j.jcmgh.2018.08.001

Müller, T., M.W. Hess, N. Schiefermeier, K. Pfaller, H.L. Ebner, P. Heinz-Erian, H. Ponstingl, J. Partsch, B. Röllinghoff, H. Köhler, et al. 2008. MYO5B mutations cause microvillus inclusion disease and disrupt epithelial cell polarity. *Nat. Genet.* 40:1163–1165. https://doi.org/10.1038/ng.225

Nicholson-Fish, J.C., A.C. Kokotos, T.H. Gillingwater, K.J. Smillie, and M.A. Cousin. 2015. VAMP4 Is an Essential Cargo Molecule for Activity-Dependent Bulk Endocytosis. *Neuron.* 88:973–984. https://doi.org/10.1016/j.neuron.2015.10.043

Nicholson-Fish, J.C., K.J. Smillie, and M.A. Cousin. 2016. Monitoring activity-dependent bulk endocytosis with the genetically-encoded reporter VAMP4-pHluorin. *J. Neurosci. Methods.* 266:1–10. https://doi.org/10.1016/j.jneumeth.2016.03.011

Pagel, J., K. Beutel, K. Lehmberg, F. Koch, A. Maul-Pavicic, A.K. Rohlfs, A. Al-Jefri, R. Beier, L. Bomme Ousager, K. Ehlert, et al. 2012. Distinct mutations in STXBP2 are associated with variable clinical presentations in patients with familial hemophagocytic lymphohistiocytosis type 5 (FHL5). *Blood.* 119:6016–6024. https://doi.org/10.1182/blood-2011-12-398958

Pohl, J.F., M.D. Shub, E.E. Trevelline, K. Ingebo, G. Silber, N. Rayhorn, S. Holve, and D. Hu. 1999. A cluster of microvillous inclusion disease in the Navajo population. *J. Pediatr.* 134:103–106. https://doi.org/10.1016/S0022-3476(99)70380-X

Qualmann, B., and R.B. Kelly. 2000. Syndapin isoforms participate in receptor-mediated endocytosis and actin organization. *J. Cell Biol.* 148: 1047–1062. https://doi.org/10.1083/jcb.148.5.1047

Qualmann, B., J. Roos, P.J. DiGregorio, and R.B. Kelly. 1999. Syndapin I, a synaptic dynamin-binding protein that associates with the neural Wiskott-Aldrich syndrome protein. *Mol. Biol. Cell.* 10:501–513. https://doi.org/10.1091/mbc.10.2.501

Rao, Y., Q. Ma, A. Vahedi-Faridi, A. Sundborger, A. Pechstein, D. Puchkov, L. Luo, O. Shupliakov, W. Saenger, and V. Haucke. 2010. Molecular basis for SH3 domain regulation of F-BAR-mediated membrane deformation. *Proc. Natl. Acad. Sci. USA.* 107:8213–8218. https://doi.org/10.1073/pnas.1003478107

Reinshagen, K., H.Y. Naim, and K.P. Zimmer. 2002. Autophagocytosis of the apical membrane in microvillus inclusion disease. *Gut.* 51:514–521. https://doi.org/10.1136/gut.51.4.514

Richards, D.A., C. Guatimosim, and W.J. Betz. 2000. Two endocytic recycling routes selectively fill two vesicle pools in frog motor nerve terminals. *Neuron.* 27:551–559. https://doi.org/10.1016/S0896-6273(00)00065-9

Ritter, B., J. Modregger, M. Paulsson, and M. Plomann. 1999. PACSIN 2, a novel member of the PACSIN family of cytoplasmic adapter proteins. *FEBS Lett.* 454:356–362. https://doi.org/10.1016/S0014-5793(99)00830-3

Rizzoli, S.O., and W.J. Betz. 2005. Synaptic vesicle pools. *Nat. Rev. Neurosci.* 6: 57–69. https://doi.org/10.1038/nrn1583

Roos, J., and R.B. Kelly. 1998. Dap160, a neural-specific Eps15 homology and multiple SH3 domain-containing protein that interacts with Drosophila dynamin. *J. Biol. Chem.* 273:19108–19119. https://doi.org/10.1074/jbc.273.30.19108

Royle, S.J., and L. Lagnado. 2003. Endocytosis at the synaptic terminal. *J. Physiol.* 553:345–355. https://doi.org/10.1113/jphysiol.2003.049221

Ruemmele, F.M., J. Schmitz, and O. Goulet. 2006. Microvillous inclusion disease (microvillous atrophy). *Orphanet J. Rare Dis.* 1:22. https://doi.org/10.1186/1750-1172-1-22

Ruemmele, F.M., T. Müller, N. Schiefermeier, H.L. Ebner, S. Lechner, K. Pfaller, C.E. Thöni, O. Goulet, F. Lacaille, J. Schmitz, et al. 2010. Loss-of-function of MYO5B is the main cause of microvillus inclusion disease: 15 novel mutations and a CaCo-2 RNAi cell model. *Hum. Mutat.* 31:544–551. https://doi.org/10.1002/humu.21224

Saeed, M.F., A.A. Kolokoltsov, T. Albrecht, and R.A. Davey. 2010. Cellular entry of ebola virus involves uptake by a macropinocytosis-like mechanism and subsequent trafficking through early and late endosomes. *PLoS Pathog.* 6:e1001110. https://doi.org/10.1371/journal.ppat.1001110

Sato, T., S. Mushiake, Y. Kato, K. Sato, M. Sato, N. Takeda, K. Ozono, K. Miki, Y. Kubo, A. Tsuji, et al. 2007. The Rab8 GTPase regulates apical protein localization in intestinal cells. *Nature.* 448:366–369. https://doi.org/10.1038/nature05929

Schneeberger, K., G.F. Vogel, H. Teunissen, D.D. van Ommen, H. Begthel, L. El Bouazzaoui, A.H. van Vugt, J.M. Beekman, J. Klumperman, T. Müller, et al. 2015. An inducible mouse model for microvillus inclusion disease reveals a role for myosin Vb in apical and basolateral trafficking. *Proc. Natl. Acad. Sci. USA.* 112:12408–12413. https://doi.org/10.1073/pnas.1516672112

Sidhaye, J., C.S. Pinto, S. Dharap, T. Jacob, S. Bhargava, and M. Sonawane. 2016. The zebrafish goosepimples/myosin Vb mutant exhibits cellular attributes of human microvillus inclusion disease. *Mech. Dev.* 142:62–74. https://doi.org/10.1016/j.mod.2016.08.001

Siminoski, K., P. Gonnella, J. Bernanke, L. Owen, M. Neutra, and R.A. Murphy. 1986. Uptake and transepithelial transport of nerve growth factor in suckling rat ileum. *J. Cell Biol.* 103:1979–1990. https://doi.org/10.1083/jcb.103.5.1979

Simpson, F., N.K. Hussain, B. Qualmann, R.B. Kelly, B.K. Kay, P.S. McPherson, and S.L. Schmid. 1999. SH3-domain-containing proteins function at distinct steps in clathrin-coated vesicle formation. *Nat. Cell Biol.* 1: 119–124. https://doi.org/10.1038/10091

Sonal, J. Sidhaye, M. Phatak, S. Banerjee, A. Mulay, O. Deshpande, S. Bhide, T. Jacob, I. Gehring, C. Nuesslein-Volhard, and M. Sonawane. 2014. Myosin Vb mediated plasma membrane homeostasis regulates peridermal cell size and maintains tissue homeostasis in the zebrafish epidermis. *PLoS Genet.* 10:. https://doi.org/10.1371/journal.pgen.1004614

Stepensky, P., J. Bartram, T.F. Barth, K. Lehmberg, P. Walther, K. Amann, A.D. Philips, O. Beringer, U. Zur Stadt, A. Schulz, et al. 2013. Persistent defective membrane trafficking in epithelial cells of patients with familial hemophagocytic lymphohistiocytosis type 5 due to STXBP2/MUNC18-2 mutations. *Pediatr. Blood Cancer.* 60:1215–1222. https://doi.org/10.1002/pbc.24475

Szperl, A.M., M.R. Golachowska, M. Bruinenberg, R. Prekeris, A.M. Thunnissen, A. Karrenbeld, G. Dijkstra, D. Hoekstra, D. Mercer, J. Ksiazyk, et al. 2011. Functional characterization of mutations in the myosin Vb gene associated with microvillus inclusion disease. *J. Pediatr. Gastroenterol. Nutr.* 52:307–313. https://doi.org/10.1097/MPG.0b013e3181eea177

Takei, K., O. Mundigl, L. Daniell, and P. De Camilli. 1996. The synaptic vesicle cycle: a single vesicle budding step involving clathrin and dynamin. *J. Cell Biol.* 133:1237–1250. https://doi.org/10.1083/jcb.133.6.1237

Uhlén, M., L. Fagerberg, B.M. Hallström, C. Lindskog, P. Oksvold, A. Mardinoglu, Å. Sivertsson, C. Kampf, E. Sjöstedt, A. Asplund, et al. 2015. Tissue-based map of the human proteome. *Science.* 347:1260419. https://doi.org/10.1126/science.1260419

Vogel, G.F., J.M. van Rijn, I.M. Krainer, A.R. Janecke, C. Posovszky, M. Cohen, C. Searle, P. Jantchou, J.C. Escher, N. Patey, et al. 2017. Disrupted apical exocytosis of cargo vesicles causes enteropathy in FHL5 patients with Munc18-2 mutations. *JCI Insight.* 2:e94564. https://doi.org/10.1172/jci.insight.94564

Weis, V.G., B.C. Knowles, E. Choi, A.E. Goldstein, J.A. Williams, E.H. Manning, J.T. Roland, L.A. Lapierre, and J.R. Goldenring. 2016. Loss of MYO5B in mice recapitulates Microvillus Inclusion Disease and reveals an apical trafficking pathway distinct to neonatal duodenum. *Cell. Mol. Gastroenterol. Hepatol.* 2:131–157. https://doi.org/10.1016/j.jcmgh.2015.11.009

Wilson, J.M., J.A. Whitney, and M.R. Neutra. 1987. Identification of an endosomal antigen specific to absorptive cells of suckling rat ileum. *J. Cell Biol.* 105:691–703. https://doi.org/10.1083/jcb.105.2.691

Wilson, J.M., J.A. Whitney, and M.R. Neutra. 1991. Biogenesis of the apical endosome-lysosome complex during differentiation of absorptive epithelial cells in rat ileum. *J. Cell Sci.* 100:133–143.

Wissig, S.L., and D.O. Graney. 1968. Membrane modifications in the apical endocytic complex of ileal epithelial cells. *J. Cell Biol.* 39:564–579. https://doi.org/10.1083/jcb.39.3.564

Wu, L.G., T.A. Ryan, and L. Lagnado. 2007. Modes of vesicle retrieval at ribbon synapses, calyx-type synapses, and small central synapses. *J. Neurosci.* 27:11793–11802. https://doi.org/10.1523/JNEUROSCI.3471-07.2007